

Attosecond physics hidden in Cherenkov radiation

D. Karlovets*, A. Chaikovsakaia, D. Grosman, D. Kargina, and G. Sizykh

School of Physics and Engineering, ITMO University, 197101 St. Petersburg, Russia

November 25, 2024

Abstract

Cherenkov radiation of charged particles moving with superluminal velocities in transparent media is a well-studied phenomenon with a plethora of applications. Its microscopic origins can be traced to the polarization of atomic shells, characterized by time scales in the subfemtosecond range — dynamics that eludes conventional macroscopic treatment. Here we present a theoretical framework for probing the intrinsic dynamics of Cherenkov radiation, unveiling quantum features absent in classical realm and even in a fully quantum theory in momentum space. These features include a finite formation length and spreading time of the photon, the latter becoming negative nearby the Cherenkov angle, a finite flash duration tied to the size of the electron packet, along with a shift in the photon arrival time that can be either positive or negative. The calculated time scales naturally lie in the attosecond range for relevant parameters, thereby linking this macroscopic phenomenon back to its atomic origins. Finally, we propose that by measuring the duration of the Cherenkov flash one can in principle retrieve the length of the emitting packet, deepening our understanding of quantum coherence effects in photon emission.

Introduction

Cherenkov radiation (ChR) by charged particles in media [1–10] is the simplest example of a wide range of phenomena embracing transition, diffraction, Smith-Purcell radiation, and other mechanisms of photon emission [11–14]. Their common microscopic origin is atomic bremsstrahlung [15] due to dynamic polarization of atomic shells by the field of the charge, and the characteristic time scales are femto- and attoseconds, typical for the AC Stark effect [16]. Along with numerous applications of classical ChR in particle detection [17], neutrino telescopes [18, 19], in gamma-ray astronomy [20, 21], and other fields, it has also recently attracted attention of biomedical community as a new tool for molecular imaging and therapy in cancer treatment [22–24]. However, despite the growing interest to inherently quantum features of ChR [25–27], a solid link between microscopic and macroscopic theories remains elusive, and the atomic dynamics stays hidden even in the fully quantum treatment of ChR in momentum space.

Here we point out that one can access atomic time scales in ChR and in its generalizations by using a quantum theory in phase space where – similar to quantum optics [28] – we employ a Wigner function to characterize the emitted photon field. We demonstrate how to probe the field in the pre-wave (or formation) zone [12, 29, 30] in which the partial waves interfere, spread, and the Cherenkov cone is not formed yet. Most strikingly, our theory establishes a link between the evolving coherence length of the electron packet, the Cherenkov flash duration, and a quantum temporal delay that the photon experiences in medium. This delay can be either positive or negative and belongs to the attosecond range, typical for atomic excitation processes studied by the attosecond spectroscopy and metrology [31]. The quantum shift in the photon arrival time, coupled with the finite flash duration and the spreading dynamics, unveils intricate coherence properties that enable refined temporal control in quantum emission processes, enriching the landscape of quantum optics, ultrafast physics, and of applications of ChR and related phenomena. The system of units $\hbar = c = 1$ is used, the electron velocity is $\beta = u_p/c \equiv u_p$, $m = 0.511$ MeV is the electron mass, $1/m \equiv \hbar/mc = 3.86 \times 10^{-11}$ cm, and $t_c = 1/m \equiv \hbar/mc^2 \approx 1.3 \times 10^{-21}$ s.

*dmitry.karlovets@metalab.ifmo.ru

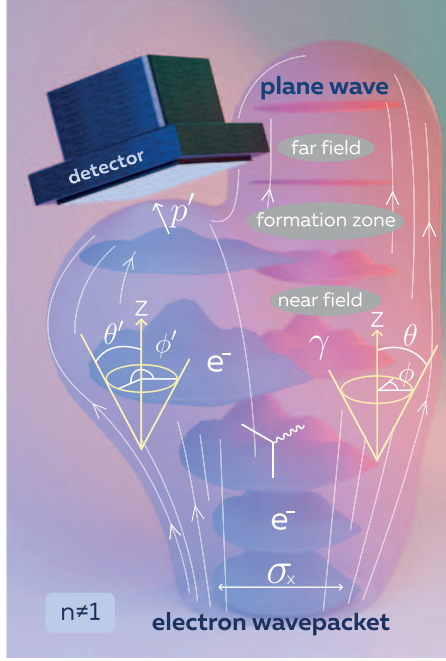


Figure 1: Generation of Cherenkov radiation by an electron packet with an rms size σ_x in a dielectric medium with a refractive index n . The photon field gradually becomes separated from the electron in the formation zone and spreads. The Cherenkov cone is formed in the far-field only if the electron is not detected. The phase space picture implies that the photon with a momentum \mathbf{k} is detected in a region of space centered at the point \mathbf{r} at the moment of time t .

Photon emission in phase space

When an electron emits a photon, the two-particle state within the first order of the perturbation theory is $|e', \gamma\rangle = (\hat{1} + \hat{S}^{(1)})|\text{in}\rangle$, where $|\text{in}\rangle = |e_{\text{in}}\rangle \otimes |0_\gamma\rangle$ and $\hat{S}^{(1)} = -ie \int d^4x \hat{j}^\mu(x) \hat{A}_\mu(x)$ [32]. Fig.1 illustrates how the photon packet gradually becomes spatially separated from the electron, spreads, and eventually turns into a plane wave propagating at the angles θ, ϕ . If we detect the electron in a plane-wave state $\langle \mathbf{p}', \lambda' |$, $\lambda' = \pm 1/2$, the state of the photon becomes

$$|\gamma\rangle = \langle \mathbf{p}', \lambda' | e_{\text{in}} \rangle |0_\gamma\rangle + \sum_{\lambda_\gamma} \int \frac{d^3k}{(2\pi)^3} |\mathbf{k}, \lambda_\gamma\rangle S_{fi}. \quad (1)$$

The second term here is a coherent superposition of plane waves with the momenta \mathbf{k} and the helicity $\lambda_\gamma = \pm 1$ and a matrix element is $S_{fi} = \langle \mathbf{k}, \lambda_\gamma; \mathbf{p}', \lambda' | \hat{S}^{(1)} | \text{in} \rangle$. We treat the incoming electron as a Gaussian packet with a wave function $f_e^{(\text{in})}(\mathbf{p}, \lambda) = \langle \mathbf{p}, \lambda | e_{\text{in}} \rangle$, a mean momentum $\langle \mathbf{p} \rangle$, an uncertainty $\sigma \ll m$, which means that the rms size – also called coherence length – of the packet is much larger than the Compton wavelength, $\sigma_x = 1/\sigma \gg 1/m$. For the moment, we take a simplified model with the packet, spherically symmetric in the laboratory frame, $\sigma_\perp = \sigma_\parallel \equiv \sigma_x = 1/\sigma$.

Let us define the energy density of the photon field in real space and time, an electric part of which is (Sec.1,2 in Supplementary)

$$\frac{1}{8\pi} \langle \gamma | \hat{\mathbf{E}}^2(\mathbf{r}, t) | \gamma \rangle \rightarrow \frac{1}{4\pi} \left| \langle 0 | \hat{\mathbf{E}}(\mathbf{r}, t) | \gamma \rangle \right|^2 = \int \frac{d^3k}{(2\pi)^3} \mathcal{W}(\mathbf{r}, \mathbf{k}, t), \quad (2)$$

where we have subtracted a contribution of the vacuum energy and $\hat{\mathbf{E}}(\mathbf{r}, t)$ is a secondary-quantized electric field operator [33]. A contribution of the magnetic field can be written similarly. Here

$$\mathcal{W}(\mathbf{r}, \mathbf{k}, t) = \frac{1}{4\pi} \sum_{\lambda_\gamma, \tilde{\lambda}_\gamma} \int \frac{d^3\tilde{k}}{(2\pi)^3} \mathbf{E}_{\tilde{\lambda}_\gamma}^*(\mathbf{k} - \tilde{\mathbf{k}}/2) \cdot \mathbf{E}_{\lambda_\gamma}(\mathbf{k} + \tilde{\mathbf{k}}/2) e^{-it(\omega(\mathbf{k}+\tilde{\mathbf{k}}/2) - \omega(\mathbf{k}-\tilde{\mathbf{k}}/2)) + i\mathbf{r} \cdot \tilde{\mathbf{k}}} \quad (3)$$

is a Wigner function of the photon, $\mathbf{E}_{\lambda_\gamma}(\mathbf{k}) = \frac{i\omega\sqrt{4\pi}}{\sqrt{2\omega n^2}} \mathbf{e}_{\mathbf{k}\lambda_\gamma} \sum_\lambda \int \frac{d^3p}{(2\pi)^3} f_e^{(\text{in})}(\mathbf{p}, \lambda) S_{fi}^{(\text{pw})}$, $\mathbf{e}_{\mathbf{k}\lambda_\gamma} \cdot \mathbf{k} = 0$, is a positive-frequency component of its electric field.

According to the standard interpretation [33], the energy density (2) defines probability to detect a photon in a region of space centered at the point \mathbf{r} at the moment of time t . Clearly, the second marginal distribution $\int d^3x \mathcal{W}(\mathbf{r}, \mathbf{k}, t) \propto |S_{fi}^{(\text{pw})}|^2$ yields probability to detect a photon with the frequency ω and a wave vector \mathbf{k} , $|\mathbf{k}| = n(\omega)\omega$, the standard result of the quantum theory in momentum space (see [26]). Therefore, it is this Wigner function (3) in phase space that contains all the information on spatial distribution of the photon field at a given distance \mathbf{r} – also in the near-field zone – and on its dynamics. Consequently, emission takes place in the pre-wave zone even if the condition of ChR is *not* met, but the waves do not constructively interfere to form a cone in the far field.

We calculate the Wigner function in the paraxial approximation, $\sigma \ll m$, in a medium with *weak dispersion*, $\frac{\omega}{n(\omega)} \frac{dn(\omega)}{d\omega} \ll 1$, and represent the amplitude [26, 32] as follows:

$$S_{fi}^{(\text{pw})} = |S_{fi}^{(\text{pw})}| e^{i\zeta_{fi}}. \quad (4)$$

Here $|S_{fi}^{(\text{pw})}|^2$ defines the emission rate in momentum space where the phase [34–36] ζ_{fi} does *not* contribute to the probability, although it is non-vanishing even in the lowest order of the perturbation theory (Sec.5 in Supplementary). The result of the calculations is (Sec.3 in Supplementary)

$$\mathcal{W}(\mathbf{r}, \mathbf{k}, t) \propto \int_0^\infty dt' \frac{e^{-R^2/R_{\text{eff}}^2(t')}}{G(t')} \cos(F(t')), \quad (5)$$

where $G(t') > 0$ is not important for now, the momentum conservation $\mathbf{p} = \mathbf{p}' + \mathbf{k}$ is implied, and

$$\mathbf{R} = \mathbf{r} - \mathbf{u}_p t + (\partial_{\mathbf{p}} + \partial_{\mathbf{k}})\zeta_{fi}(\mathbf{p}, \lambda_e, \mathbf{k}, \lambda_\gamma). \quad (6)$$

Here $\mathbf{u}_p = \mathbf{p}/\varepsilon(\mathbf{p})$, $\varepsilon(\mathbf{p}) = \sqrt{\mathbf{p}^2 + m^2}$, $\mathbf{u}_k = \mathbf{k}/(n|\mathbf{k}|)$, $|\mathbf{u}_k| = 1/n$, $F(t') \propto \arctan t'/t_d$ contains a Gouy phase of the photon connected to its spreading with time t' , and t_d is a diffraction time (see below).

The principal behavior of the Wigner function (5), which is *not* everywhere positive, is governed by the ratio

$$\frac{R^2}{R_{\text{eff}}^2(t')} = \frac{1}{\sigma_x^2(t')} \left(\underbrace{\frac{[\mathbf{R} \times (\mathbf{u}_p - \mathbf{u}_k)]^2}{(\mathbf{u}_p - \mathbf{u}_k)^2}}_{\text{finite at } t' = 0} + \text{terms vanishing at } t' = 0 \right), \quad (7)$$

where $\sigma_x^2(t') = \sigma^{-2} (1 + (t'/t_d)^2)$ is an rms size of the electron packet. When the condition of ChR is met, $u_p > u_k$, the vector $\mathbf{u}_k - \mathbf{u}_p$ is directed backwards with respect to the electron velocity \mathbf{u}_p , and dependence of the Wigner function on \mathbf{R} at small t' vanishes along $\mathbf{u}_k - \mathbf{u}_p$, defining *the Mach cone* with an angle

$$\theta_{\text{Mach}} = \pi - \arcsin \left(\frac{\sin \theta}{n|\mathbf{u}_k - \mathbf{u}_p|} \right). \quad (8)$$

If the electron is detected in a plane-wave state, scattered at the angles θ' , ϕ' , the radius $R_{\text{eff}}(t')$ depends on the difference $\phi_R - \phi$ between the azimuthal angle of \mathbf{R} and that of \mathbf{k} , so it is *anisotropic*. The azimuthal symmetry of the Mach cone is restored when the electron is *not* detected and we integrate Eq.(5) over \mathbf{p}' .

At large t' , we find $R_{\text{eff}}^2(t') \propto \sigma_x^2(0) t'^2/t_d^2$ and when $R_{\text{eff}}(t') \gg R$ dependence of the Wigner function on \mathbf{r} and t *vanishes*, whereas in the other limiting case, $R \gg R_{\text{eff}}(t')$, it is exponentially suppressed. So, an effective region of space-time correlation is when $t' \lesssim t_d$, and $R \sim R_{\text{eff}}(t')$ is where it is most pronounced, which is why one can call $R_{\text{eff}}(t')$ *the correlation radius*. At $t' \gg t_d$, both the electron packet and the photon field spread and so there is no longer space-time correlation within the region $R < R_{\text{eff}}(t')$, which is a hallmark of the wave zone. We show in Fig.2 that the correlation radius is orders of magnitude *smaller* than the distance $u_p t'$ traveled by the electron for all the angles θ_R of \mathbf{R} , except for the Mach angle, $\theta_R \approx \theta_{\text{Mach}}$ (shown in Fig.3 c.).

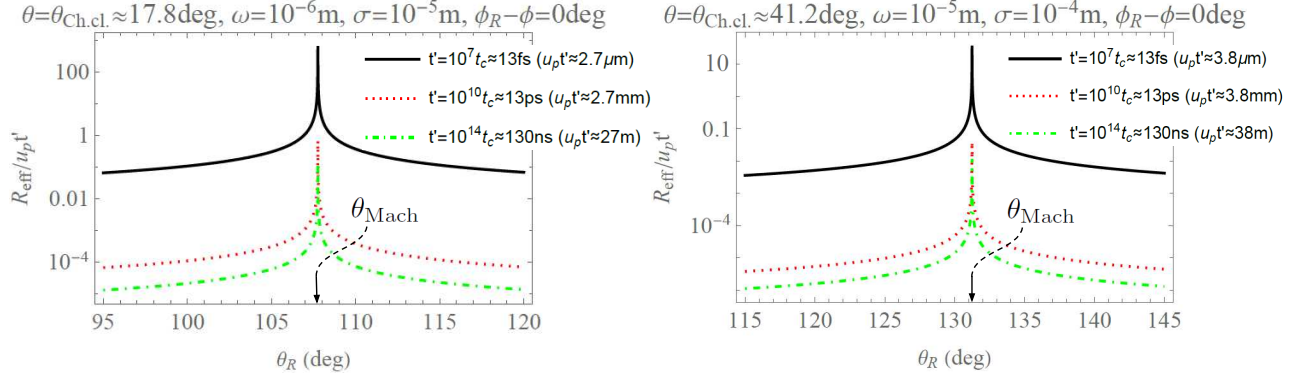


Figure 2: The effective correlation radius from Eq.(7) divided by the distance $u_p t'$ traveled by the electron during the time t' . Left: $\beta = 0.7$ ($\gamma = 1.4$), $n = 1.5$, $\theta_{\text{Ch.cl.}} = \arccos 1/u_p n \approx 17.8$ deg, $\theta_{\text{Mach}} \approx 107.8$ deg. Right: $\beta = 0.9999$ ($\gamma = 70.7$), $n = 1.33$, $\theta_{\text{Ch.cl.}} \approx 41.2$ deg, $\theta_{\text{Mach}} \approx 131.2$ deg. Nearby the Mach angle, space-time dependence of the Wigner function quickly vanishes within the correlation radius $R < R_{\text{eff}}(t')$.

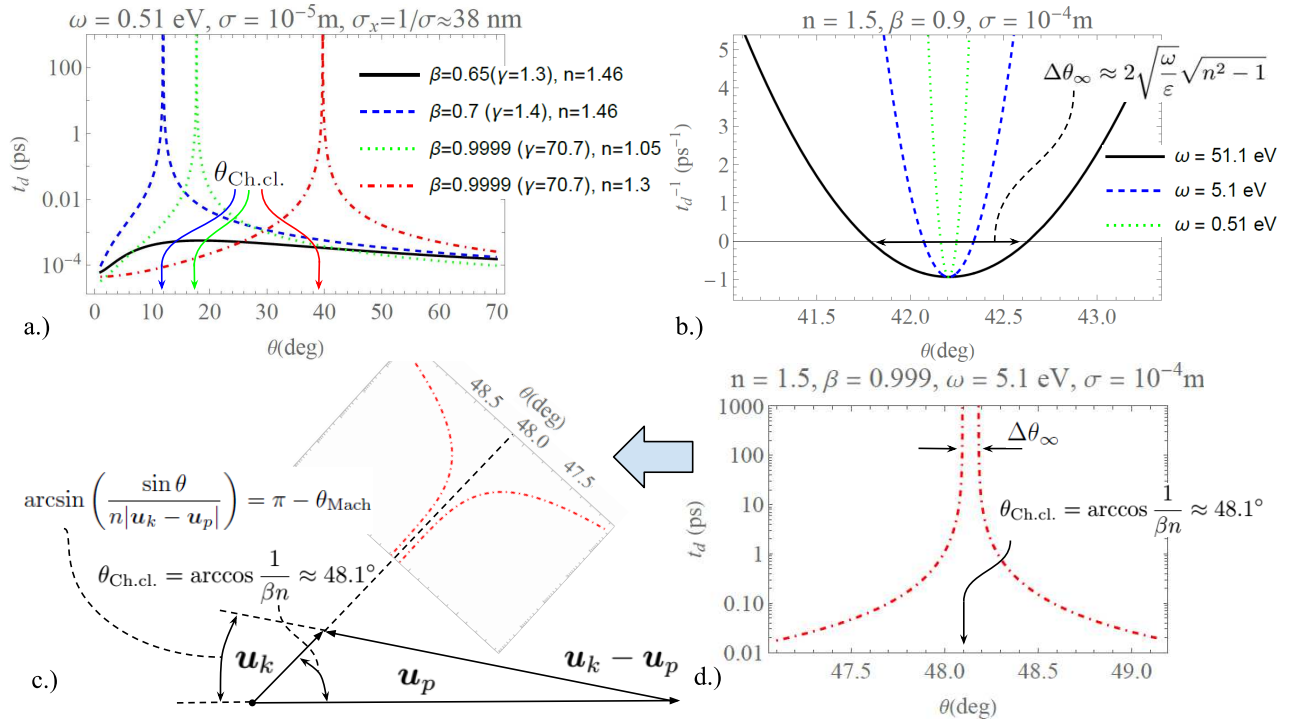


Figure 3: The spreading time (9) of the photon field measured in picoseconds (a. and d.) and its inverse (b.). The sharp maxima are nearby the angle $\theta_{\text{Ch.cl.}} = \arccos 1/u_p n$. The Cherenkov condition is *not* met for the black line in a.), which is why the photon field quickly spreads during hundreds of attoseconds. The right upper panel shows two points (10), between which the spreading time turns negative due to the quantum recoil ($\omega/\varepsilon \neq 0$, see Eq.(11)).

Spreading time and formation length

Let us discuss now the spreading time, which is found as

$$t_d = \frac{2}{\sigma^2} \frac{(\mathbf{u}_p - \mathbf{u}_k)^2}{(1/\omega n^2 - \varepsilon^{-1})(\mathbf{u}_p - \mathbf{u}_k)^2 + (\varepsilon^{-1} - \omega^{-1})[\mathbf{u}_p \times \mathbf{u}_k]^2}. \quad (9)$$

where $(\mathbf{u}_p - \mathbf{u}_k)^2 = n^{-2} + u_p^2 - 2u_p \cos \theta/n$, $[\mathbf{u}_p \times \mathbf{u}_k]^2 = u_p^2 \sin^2 \theta/n^2$ with the z axis directed along the electron partial momentum \mathbf{p} . One can also define *the formation length* of radiation as $L_f = u_p |t_d|$, which turns to infinity at the Cherenkov angle in the classical Tamm problem [11, 12, 37, 38].

The diffraction time and the formation length have an extremum either at the angle $\cos \theta_{\text{Ch.cl.}} = 1/u_p n < 1$, when the Cherenkov condition $u_p > 1/n$ is met, or at $\cos \theta = u_p n < 1$ otherwise. Importantly, the Wigner function and the energy density stay finite in the latter case, but the photon field rapidly spreads (see the black line in Fig.3 a.)). Along with the extremum, the time t_d has two points in which its denominator *vanishes* (see Fig.3 b.)),

$$\cos \theta_\infty \approx \frac{1}{u_p n} \left(1 \mp \sqrt{\frac{\omega}{\varepsilon} \sqrt{(n^2 - 1)(u_p^2 n^2 - 1)}} \right), \quad (10)$$

where we have kept the first correction due to quantum recoil, which is usually very small [26], $\omega/\varepsilon \ll 1$. Clearly, the diffraction time can only turn to infinity under the condition of ChR, $u_p n > 1$. The angular width between the two points is

$$\Delta \theta_\infty \approx 2 \sqrt{\frac{\omega}{\varepsilon} \sqrt{n^2 - 1}}, \quad (11)$$

and it vanishes for classical emission with no recoil, $\omega/\varepsilon \rightarrow 0$. For materials like Al, Si, Be, and Ti, Cherenkov radiation can be observed in the soft X-ray range at the frequencies [38–40] $\omega \approx 72.5, 100, 110, 453.8$ eV, respectively, which for $\varepsilon \sim (5 - 20)m$ yields $\Delta \theta_\infty < 1 - 2$ deg (cf. Fig.3 c.), d.)).

Between the above points, the time t_d becomes *negative* – see Fig.3 b.) – and the Gouy phase $\arctan t'/t_d$ changes its sign, as if the electron packet *shrinks* during the emission. In the classical regime with no recoil, both the points merge and so t_d and L_f turn to infinity at the Cherenkov angle. Indeed, in a vicinity of this angle the spreading time with the recoil kept is

$$t_d \Big|_{\cos \theta = 1/nu_p} = \frac{2\varepsilon}{\sigma^2} \frac{n^2}{1 - n^2} < 0, \quad (12)$$

where $\varepsilon = \gamma m$. We compare this with the spreading time of an electron packet, which is at rest on average in vacuum [41] $t_d^{(e, \text{rest})} = m/\sigma^2$. In the laboratory frame this time is γ times larger, which coincides with $|t_d|$ up to the factor $2n^2/(n^2 - 1) > 2$. So, in a vicinity of the Cherenkov direction spreading of the photon *seems to reverse back* and it is intimately connected with spreading of the electron packet.

The coherence lengths of non-relativistic electrons amount to $\sigma_x(0) \sim 1 - 10$ nm nearby the generation region for standard sources like cathodes of the electron guns in accelerators or electron microscopes [41–45]. These estimates can likewise be obtained by using the emission duration of photo-electrons from a tungsten tip [46] for which the measured sub-femtosecond duration yields nanometer-sized packets. Therefore for $\gamma \gtrsim 1 - 2, n \gtrsim 1$ the electron spreading time is $t_d^{(e)} \gtrsim 10^{-2} - 10$ ps, and the time t_d for the photon nearby the Cherenkov angle is of the same order of magnitude, see Fig.3. The time of flight of an electron through a target of a few centimeters in length is roughly 0.1 ns, and therefore spreading of the electron *can* be important even not far from $\theta_{\text{Ch.cl.}}$, especially for large Cherenkov generators employed, for instance, in neutrino telescopes, except for ultrarelativistic particles with $\gamma \gg 1$.

Shift of the photon arrival time and flash duration

Dependence of the Wigner function (5) on the detection time t comes exclusively from the following envelope:

$$\exp \left\{ -\frac{R^2}{R_{\text{eff}}^2(t')} \right\} \propto \exp \left\{ -\frac{(t - t_0)^2}{2\sigma_t^2(t')} \right\},$$

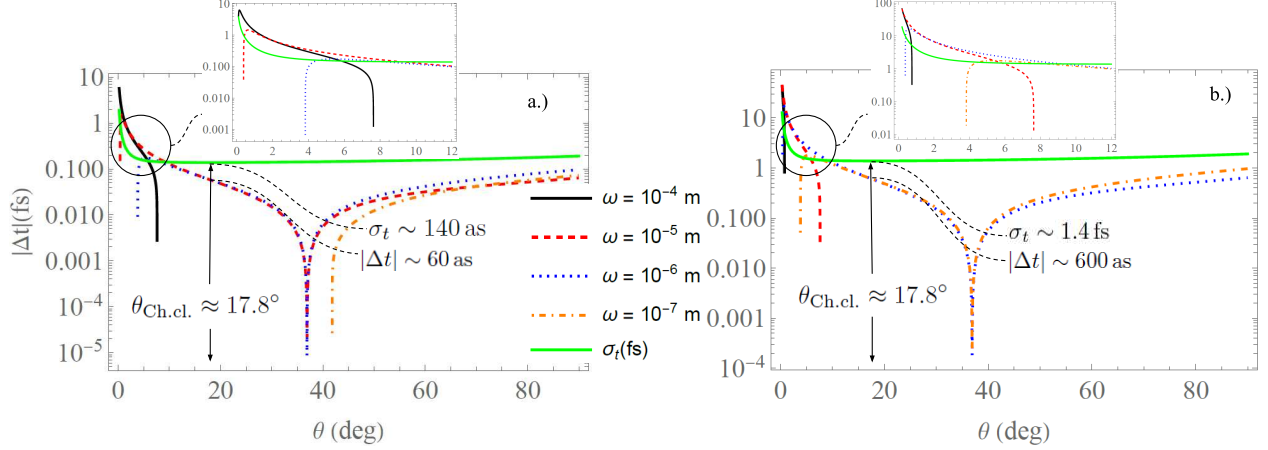


Figure 4: The quantum shift $\Delta t = t_0 - t_{\text{cl.}} = \mathbf{l}_0 \cdot (\partial_{\mathbf{p}} + \partial_{\mathbf{k}})\zeta_{fi}$ from Eq.(15) of the photon arrival time compared to the classical value and the Cherenkov flash duration (the green lines with $\sigma = p_{\perp}$). The electron energy is typical for a transmission electron microscope: $\beta = 0.7$, and $p'_{\perp} = 0.99 \times p_{\perp}$, $p'_z = 0.9 \times \beta$, $n = 1.5$. The left panel (a.): $p_{\perp} = 10^{-5} m$, $1/p_{\perp} \gtrsim 10$ nm, the right panel (b.): $p_{\perp} = 10^{-6} m$, $1/p_{\perp} \gtrsim 100$ nm. The behaviour at small angles is shown in the insets. The shifts vanish in those regions that are not allowed by the momentum conservation law, they stay roughly the same for other p'_{\perp}, p'_z and for ultrarelativistic electrons, $\gamma \gg 1$, though the Cherenkov angle grows.

$$\sigma_t^2(t') = \frac{\sigma_x^2(t') (\mathbf{u}_p - \mathbf{u}_k)^2}{2 [\mathbf{u}_p \times \mathbf{u}_k]^2}. \quad (13)$$

Here natural duration of the Cherenkov flash is defined by $\sigma_t(t')$ and a time instant at which the probability to catch the photon around the point \mathbf{r} is maximized is $t_0 = \mathbf{l}_0 \cdot (\mathbf{r} + (\partial_{\mathbf{p}} + \partial_{\mathbf{k}})\zeta_{fi})$, $\mathbf{l}_0 = [(\mathbf{u}_p - \mathbf{u}_k) \times [\mathbf{u}_k \times \mathbf{u}_p]] / [\mathbf{u}_p \times \mathbf{u}_k]^2$.

One can neglect the term with the phase ζ_{fi} in \mathbf{R} (6) in the wave zone where $r \rightarrow \infty$, and then the Wigner function (5) and the emitted energy are concentrated in a vicinity of the electron classical trajectory [47], $\mathbf{r} \sim \mathbf{u}_p t$. The detector registers a photon in the far field emitted at $t = 0, r_0 = 0$ by a classical point-like electron at the time instant

$$t_{\text{cl.}}^{(\text{far-f.})} = r/u_k = r n, \quad (14)$$

which will be called the classical arrival time. Let us compare this prediction with the above t_0 , derived quantum mechanically. Directing the z axis along the electron momentum \mathbf{p} , we find $\mathbf{k} = n\omega\mathbf{l}$, $\mathbf{l} = \{\sin\theta \cos\phi, \sin\theta \sin\phi, \cos\theta\}$, $r \equiv \mathbf{r} \cdot \mathbf{l}$, $t_{\text{cl.}}^{(\text{far-f.})} = \mathbf{r} \cdot \mathbf{l} n$, and $\mathbf{l}_0 = \sin^{-2}\theta ((u_p^{-1} - n \cos\theta) \mathbf{p}/|\mathbf{p}| + (n - u_p^{-1} \cos\theta) \mathbf{l})$. In a vicinity of the Cherenkov angle, we have $\mathbf{l}_0 \rightarrow \mathbf{l} n$ and so for $\zeta_{fi} = 0$ we get $t_0 \rightarrow t_{\text{cl.}}^{(\text{far-f.})} = \mathbf{r} \cdot \mathbf{l} n$, in accord with Eq.(14).

However the phase ζ_{fi} *cannot* be ignored in the formation zone and this affects the photon arrival time t_0 . In this regime, we call $t_{\text{cl.}} = \mathbf{r} \cdot \mathbf{l}_0$ for arbitrary emission angles and so the quantum shift is

$$\Delta t = t_0 - t_{\text{cl.}} = \mathbf{l}_0 \cdot (\partial_{\mathbf{p}} + \partial_{\mathbf{k}})\zeta_{fi}. \quad (15)$$

The physical origin of this delay is the electric dipole moment density $\propto e(\partial_{\mathbf{p}} + \partial_{\mathbf{k}})\zeta_{fi}$ induced in medium by the field of the electron. We deal with an analogue of the AC Stark effect [16] with the atoms being off-resonantly polarized by a broadband spectrum $\Delta\omega$ of pseudo-photons. Similarly to the observed time delays when a laser propagates in a medium [48–50], here we encounter delays induced by the virtual photons, reemitted as real ones. Classically, one can look at this as if the photon was emitted not from a point-like electron, but from a point shifted laterally to $\Delta\rho \sim \beta\gamma\lambda/2\pi$ from its trajectory, which is a mean free path of the virtual photon [12, 29]. Numerically $\Delta\rho/c \sim \beta\gamma\lambda/2\pi c = \beta\gamma/\omega \sim 1$ fs – 100 fs for photons from IR to UV ranges and $\gamma = \varepsilon/m \sim 10$.

When measuring the quantum shift in the photon arrival time from its classical value, the flash duration $\sigma_t(t')$ is crucial because the deviations can hardly be discerned when $\sigma_t(t') \gg |\Delta t|$ occurring for $t' \gg t_d$ far from the Cherenkov angle. This duration was estimated by Frank as early as in 1956

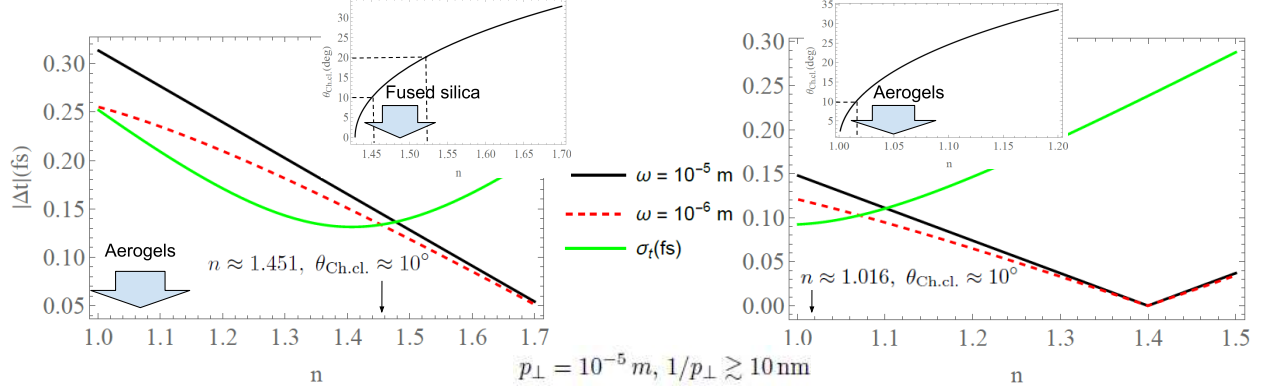


Figure 5: Dependence of the shift $\Delta t = t_0 - t_{\text{cl.}} = \mathbf{l}_0 \cdot (\partial_{\mathbf{p}} + \partial_{\mathbf{k}})\zeta_{fi}$ from Eq.(15) of the photon arrival time on the refractive index n at the emission angle $\theta = 10$ deg. Left: $\beta = 0.7, p'_z = 0.9 \times \beta$ (a TEM regime; the minimal refractive index for which the Cherenkov condition is met is $n \approx 1.429$, whereas $n = 1.45 - 1.55$ for fused silica in the given spectral range), right: $\beta = 0.9999 (\gamma = 70.7), p'_z = 0.99 \times \beta$ (an accelerator regime). The classical Cherenkov angle $\theta_{\text{Ch.cl.}} = \arccos 1/\beta n$ is shown in the insets.

from the classical considerations [8,9] to be $\sim 1/\Delta\omega < 1$ ps where $\Delta\omega$ is a frequency interval for which the emission takes place. The quantum estimates from the uncertainty principle for the off-resonant AC Stark effect yield the same result [16], $1/\Delta\omega \sim 0.1 - 100$ fs for $\Delta\omega \sim 10^{-2} - 10$ eV. Our quantum model predicts the following flash duration nearby the Cherenkov angle:

$$\sigma_t(t') \rightarrow n \sigma_x(0)/\sqrt{2}, \quad (16)$$

because in this case $t_d \rightarrow \infty$. Clearly, only the electron packet's size at the target entrance ($t' = 0$) contributes to the flash duration nearby $\theta_{\text{Ch.cl.}}$. For realistic electrons with $\sigma_x(0) \sim 1 - 100$ nm, we find

$$\sigma_t(0) \sim 10 \text{ as} - 1 \text{ fs}. \quad (17)$$

In Figures 4 and 5 we show that the typical shifts indeed belong to the attosecond range and that the flash duration is larger than the shift, except for small angles. The electron transverse momenta are chosen to be $p_{\perp} = \sigma \sim (10^{-7} - 10^{-4}) m$ because they correspond to the spatial widths $1/p_{\perp} = \sigma_x(0) \gtrsim 1 \text{ nm} - 1 \mu\text{m}$, respectively, and we also neglect the spreading. Note that within the pre-wave zone the emission does *not* take place only at the Cherenkov angle. The sign of the shift *swaps* between the two kinematic scenarios (Sec.4,5 in Supplementary), which is why the absolute value $|\Delta t|$ is shown. Fixing the detector at certain angles θ, ϕ and the distance r , one would see that the photons equally probably arrive either later (time delay) than $t_{\text{cl.}}$ or sooner than that (negative delay), if the electron is *not* detected. Note that integration of the Wigner function over \mathbf{p}' puts the electron momentum to the definite value $\mathbf{p}' = \mathbf{p} - \mathbf{k}$ with subsequent integration over \mathbf{p} with the Gaussian distribution. If one wishes to catch only the shifts with *one particular sign*, one should detect the photon and the electron in coincidence, which is technically more challenging.

In Figure 5 we highlight that the flash duration σ_t , shown with the green line, can drop below the temporal shift for angles $\theta \lesssim 10 - 15$ deg and media with small refractive indices $n \sim 1.01 - 1.5$, however, only with no spreading taken into account as $\sigma_t(t')$ grows with the time t' , whereas the shift does not. For the energies of transmission electron microscopes (TEM), $\beta \sim 0.7$, a target made of fused silica with $n = 1.458$ in the optical range can do the job, whereas for ultrarelativistic electrons, $\gamma \gg 1$, aerogels with $n \sim 1.01 - 1.3$ can be employed, which are already used as Cherenkov generators [51–53]. The use of Brewster-Cherenkov detectors [54] can also come in handy here.

If we now go beyond the model of the electron packet with $\sigma_{\perp} = \sigma_{\parallel}$ and recall that there is Lorentz contraction, $\sigma_{\parallel} = \gamma^{-1}\sigma_{\perp}$, the flash durations can become γ times *shorter* than (17). Although photon spreading can be safely neglected nearby the Cherenkov angle, spreading of the electron *before* entering the target can significantly increase these numbers. According to the quantum dynamics of the coherence length $\sigma_x(t')$ – also called the generalized van Cittert-Zernike theorem [41] – when an electron is released from a photo-gun or a field emitter with rms sizes $\sigma_{\perp} \sim \sigma_{\parallel}$ [42] of a few nanometers and an energy up to a few tens of eV, it spreads to some tens of nanometers at the distance of $1 \mu\text{m}$ and it reaches micrometer

sizes already at 1 mm. Clearly, electron acceleration – say, in an RF cavity – mitigates the spreading rate, but a realistic estimate of the packet length σ_{\parallel} at the target boundary remains *unknown*.

In practice, achieving attosecond flash durations requires electrons generating radiation with no spreading before the target, just after the emission from a cathode. A vacuum gap of even a few millimeters after the source would yield micrometer-sized electron packets entering the target, which results in picosecond durations (subpicosecond with acceleration to a few MeV) measurable by streak cameras. State-of-the-art Cherenkov counters at accelerators have picosecond time resolution [53,55], the subfemtosecond resolution can be achieved at X-ray free-electron lasers [56,57] or with the frequency-resolved optical gating [58], whereas it is nanoseconds for Cherenkov telescopes in gamma-ray astronomy [21] where spreading effects are notable. Attosecond photon pulses – including twisted photons with orbital angular momentum – are usually obtained through high-harmonic generation in the extreme-ultraviolet and even soft X-ray ranges [59,60], enabling vortex electrons generation via photoionization [60]. The ChR can be a source of twisted photons [26,61], also in the soft X-ray range, and shaping the spatial and temporal profiles of the electron wave function offers refined tuning of phase-space profile of the photons.

Close to the Cherenkov angle, the flash duration is directly tied to the electron coherence length upon entering the medium, opening avenues for controlling this duration by selecting packets of desired length and accelerating them in the low-current regime with no space-charge effects, typical for TEMs. Alternatively, measuring photon pulse durations can provide a novel method for determining electron packet length, a complementary approach to interferometry that is reminiscent of bunch length measurements via classical coherence [14]. The developed framework provides visualization of the emitted photon energy in real space and time, which is particularly desirable for biomedical applications of ChR in radiotherapy [23,24] where only the classical Tamm-Frank theory in the far field has been used so far, apparently overestimating the process intensity in the formation zone. Naturally, ChR serves as an exemplary case within a broader class of media-induced emission phenomena where attosecond time scales are accessible via the phase-space analysis.

Acknowledgment. We are grateful to D. Glazov, I. Ivanov, A. Shchepkin, V. Serbo, I. Pavlov, and especially to A. Tishchenko for useful discussions and suggestions, and also to Maria Zhuravleva for the help with the 3D picture. The studies on photon emission in phase space are supported by the Foundation for the Advancement of Theoretical Physics and Mathematics “BASIS”. Those on the temporal features of radiation at the finite distance by the Russian Science Foundation (Project No. 23-62-10026 <https://rscf.ru/en/project/23-62-10026/>). The analysis of the quantum shift is supported by the Government of the Russian Federation through the ITMO Fellowship and Professorship Program.

References

- [1] P. Cherenkov, Doklady Akad. Nauk SSSR **2**, 451 (1934).
- [2] S. Vavilov, Doklady Akad. Nauk SSSR **2**, 457 (1934).
- [3] I. Frank and I. Tamm, Doklady Akad. Nauk SSSR **14**, 107 (1937).
- [4] V. Ginzburg, Zh. Eksp. Teor. Fiz. **10**, 589 (1940).
- [5] A. Sokolov, Dokl. Akad. Nauk USSR **28**, 415 (1940).
- [6] I. Tamm, General characteristics of radiation emitted by systems moving with super-light velocities with some applications to plasma physics, <https://www.nobelprize.org/prizes/physics/1958/tamm/lecture/>, 1958, Nobel Lecture.
- [7] I. Frank, Optics of light sources moving in refractive media, <https://www.nobelprize.org/prizes/physics/1958/frank/lecture/>, 1958, Nobel Lecture.
- [8] I. M. Frank, Uspekhi Fiz. Nauk [Sov. Phys. Usp.] **58**, 111 (1956), (in Russian).
- [9] I. Frank, Nuclear Instruments and Methods in Physics Research Section A: Accelerators, Spectrometers, Detectors and Associated Equipment **248**, 7 (1986).
- [10] B. M. Bolotovskii, Phys. Usp. **52**, 1099 (2009).

- [11] V. L. Ginzburg and V. N. Tsytovich, *Transition radiation and transition scattering-some questions regarding the theory* (Nauka, 1984), [Adam Hilger, Bristol 1990].
- [12] A. P. Potylitsyn *et al.*, *Diffraction Radiation from Relativistic Particles*, STMP Vol. 239 (Springer, Berlin Heidelberg, 2010).
- [13] S. J. Smith and E. M. Purcell, *Phys. Rev.* **92**, 1069 (1953).
- [14] A. Curcio *et al.*, *Phys. Rev. Accel. Beams* **23**, 022802 (2020).
- [15] A. V. Korol and A. V. Solov'yov, *Polarization Bremsstrahlung* (Springer, 2014).
- [16] N. B. Delone and V. P. Krainov, *Physics-Uspekhi* **42**, 669 (1999).
- [17] R. Forty and O. Ullaland, *Particle Identification: Time-of-Flight, Cherenkov and Transition Radiation Detectors* (Springer International Publishing, Cham, 2020), pp. 281–335.
- [18] M. Koshiha, *Rev. Mod. Phys.* **75**, 1011 (2003).
- [19] V. A. Allakhverdyan *et al.*, *Phys. Rev. D* **107**, 042005 (2023).
- [20] E. Aliu *et al.*, *Astroparticle Physics* **30**, 293 (2009).
- [21] D. Depaoli *et al.*, *Nuclear Instruments and Methods in Physics Research Section A: Accelerators, Spectrometers, Detectors and Associated Equipment* **1060**, 169047 (2024).
- [22] D. A. Alexander *et al.*, *Light: Science & Applications* **10**, 226 (2021).
- [23] B. Cline, I. Delahunty, and J. Xie, *WIREs Nanomedicine and Nanobiotechnology* **11**, e1541 (2019).
- [24] A. K. Glaser, R. Zhang, J. M. Andreozzi, D. J. Gladstone, and B. W. Pogue, *Physics in Medicine & Biology* **60**, 6701 (2015).
- [25] I. Kammer *et al.*, *Physical Review X* **6**, 011006 (2016).
- [26] I. Ivanov, V. Serbo, and V. Zaytsev, *Physical Review A* **93**, 053825 (2016).
- [27] C. Roques-Carmes, N. Rivera, J. Joannopoulos, M. Soljačić, and I. Kammer, *Physical Review X* **8**, 041013 (2018).
- [28] W. P. Schleich, *Quantum optics in phase space* (John Wiley & Sons, 2015).
- [29] V. A. Verzilov, *Phys. Lett. A* **273**, 135 (2000).
- [30] M. Galletti *et al.*, *New Journal of Physics* **25**, 063014 (2023).
- [31] F. Krausz and M. Ivanov, *Reviews of Modern Physics* **81**, 163 (2009).
- [32] V. Berestetskii, E. Lifshitz, and L. Pitaevskii, *Quantum Electrodynamics* (Butterworth-Heinemann, 1982).
- [33] M. Scully and M. Zubairy, *Quantum optics* (Cambridge university press, 1997).
- [34] K. Bliokh *et al.*, *Physics Reports* **690**, 1 (2017).
- [35] G. Antchev *et al.*, *The European Physical Journal C* **76**, 1 (2016).
- [36] I. Ivanov, *Progress in Particle and Nuclear Physics* **127**, 103987 (2022).
- [37] V. Pafomov, *Tr. Fiz. Inst. im. P. N. Lebedeva, Ross. Akad. Nauk* **44**, 28 (1969), [Proc. P. N. Lebedev, *Phys. Inst.* 44, 25 (1971)].
- [38] M. Shevelev, A. Konkov, and A. Aryshev, *Physical Review A* **92**, 053851 (2015).
- [39] S. Uglov and A. Vukolov, *Journal of Instrumentation* **16**, P07043 (2021).

- [40] S. Uglov, A. Vukolov, V. Kaplin, L. Sukhikh, and P. Karataev, *Europhysics Letters* **118**, 34002 (2017).
- [41] D. Karlovets, *New Journal of Physics* **23**, 033048 (2021).
- [42] D. Ehberger *et al.*, *Physical Review Letters* **114**, 227601 (2015).
- [43] B. Cho, T. Ichimura, R. Shimizu, and C. Oshima, *Physical Review Letters* **92**, 246103 (2004).
- [44] T. Latychevskaia, *Ultramicroscopy* **175**, 121 (2017).
- [45] B. Cho and C. Oshima, *Bulletin of the Korean Chemical Society* **34**, 892 (2013).
- [46] P. Dienstbier *et al.*, *Nature* **616**, 702 (2023).
- [47] V. Bagrov, V. Belov, and A. Trifonov, *Journal of Physics A: Mathematical and General* **26**, 6431 (1993).
- [48] I. Jordan *et al.*, *Science* **369**, 974 (2020).
- [49] A. Sommer *et al.*, *Nature* **534**, 86 (2016).
- [50] D. Angulo *et al.*, arXiv preprint arXiv:2409.03680 (2024).
- [51] I. Adachi, M. Tabata, H. Kawai, and T. Sumiyoshi, *Nuclear Instruments and Methods in Physics Research Section A: Accelerators, Spectrometers, Detectors and Associated Equipment* **639**, 222 (2011).
- [52] A. C. Pierre, *Introduction to sol-gel processing* (Springer Nature, 2020).
- [53] O. Meshkov *et al.*, *Proc. 13th International Beam Instrumentation Conference*, 613 (2024), [THP64].
- [54] X. Lin *et al.*, *Nat. Commun.* **12**, 1 (2021).
- [55] M. Shaikh *et al.*, *Phys. Rev. Lett.* **120**, 065001 (2018).
- [56] Z. Guo *et al.*, *Nature Photonics* **18**, 691 (2024).
- [57] J. Duris *et al.*, *Nature Photonics* **14**, 30 (2020).
- [58] R. Jafari, S. D. Khosravi, and R. Trebino, *Scientific Reports* **12**, 21006 (2022).
- [59] A. de las Heras *et al.*, *Optica* **11**, 1085 (2024).
- [60] R. Géneaux *et al.*, *Nat. Commun.* **7**, 1 (2016).
- [61] D. Karlovets, S. Baturin, G. Geloni, G. Sizykh, and V. Serbo, *The European Physical Journal C* **83**, 372 (2023).

Supplementary to Attosecond physics hidden in Cherenkov radiation

D. Karlovets, A. Chaikovsakaia, D. Grosman, D. Kargina, and G. Sizykh

School of Physics and Engineering, ITMO University, 197101 St. Petersburg, Russia

November 25, 2024

1 The photon evolved state

Let us describe photon emission in QED with a final state consisting of an electron and a photon with Cherenkov radiation (ChR) in a transparent medium being specific example. A bipartite evolved state is obtained by acting on the initial state by an evolution operator within the first order of the perturbation theory [1, 2],

$$\hat{S} \approx \hat{1} + \hat{S}^{(1)} = \hat{1} - ie \int d^4x \hat{j}^\mu(x) \hat{A}_\mu(x), \quad (1)$$

where the integration over time spans from $t_i = -\infty$ to $t_f = +\infty$. So, the evolved state is

$$|e', \gamma\rangle = (\hat{1} + \hat{S}^{(1)}) |\text{in}\rangle, \quad (2)$$

where $|\text{in}\rangle = |e_{\text{in}}\rangle \otimes |0_\gamma\rangle$. One can insert a unity operator $\hat{1}_{e\gamma}$ on the two-particle space with the complete set being the plane-wave states with momenta \mathbf{p}' , \mathbf{k} and helicities $\lambda' = \pm 1/2$, $\lambda_\gamma = \pm 1$. So that

$$|e', \gamma\rangle = |\text{in}\rangle + \sum_{\lambda' = \pm 1/2, \lambda_\gamma = \pm 1} \int \frac{d^3k}{(2\pi)^3} \frac{d^3p'}{(2\pi)^3} |\mathbf{p}', \lambda'\rangle \otimes |\mathbf{k}, \lambda_\gamma\rangle S_{fi}^{(1)}. \quad (3)$$

If we now project the final electron state to a bra $\langle f_e^{(\text{det})} | = \langle \mathbf{p}', \lambda' |$, the evolved state of the final photon alone becomes

$$|\gamma\rangle = \langle \mathbf{p}', \lambda' | e_{\text{in}} \rangle |0_\gamma\rangle + \sum_{\lambda_\gamma} \int \frac{d^3k}{(2\pi)^3} |\mathbf{k}, \lambda_\gamma\rangle S_{fi}^{(1)},$$

$$S_{fi}^{(1)} \equiv S_{fi}^{(1)}(\mathbf{p}', \lambda', \mathbf{k}, \lambda_\gamma) = \langle \mathbf{k}, \lambda_\gamma; \mathbf{p}', \lambda' | \hat{S}^{(1)} | \text{in} \rangle. \quad (4)$$

The electron momentum states are on-shell with the energy $\varepsilon'_e = \sqrt{m^2 + (\mathbf{p}')^2}$. The incoming electron is described as a Gaussian packet with the following wave function:

$$f_e^{(\text{in})}(\mathbf{p}, \lambda) = \langle \mathbf{p}, \lambda | e_{\text{in}} \rangle = \delta_{\lambda, \lambda_e} \left(\frac{2\sqrt{\pi}}{\sigma} \right)^{3/2} \exp \left\{ -\frac{(\mathbf{p} - \langle \mathbf{p} \rangle)^2}{2\sigma^2} \right\}, \quad (5)$$

with $\sigma \ll m$ being the momentum uncertainty, so that $\sigma_x = 1/\sigma \gg 1/m \equiv \hbar/mc \approx 3.86 \times 10^{-11}$ cm is the electron Compton wavelength. For simplicity, we employ first the model with a symmetric packet in the laboratory frame, $\sigma_\perp = \sigma_\parallel \equiv \sigma_x = 1/\sigma$. In the main manuscript, we discuss possible changes of the predicted effects in a more realistic model with a packet, symmetric in the rest frame with $\langle \mathbf{p} \rangle = 0$, which experiences Lorentz contraction in the laboratory frame, $\sigma_\parallel = \gamma^{-1} \sigma_\perp$, where $\gamma = \sqrt{m^2 + \langle \mathbf{p} \rangle^2}/m$.

2 Spatial energy density and the Wigner function

Let us define the following Hermitian field operators:

$$\begin{aligned}
\hat{\mathbf{A}}(\mathbf{r}, t) &= \sum_{\lambda_\gamma = \pm 1} \int \frac{d^3 k}{(2\pi)^3} (\mathbf{A}_{\mathbf{k}\lambda_\gamma}(\mathbf{r}, t) \hat{c}_{\mathbf{k}\lambda_\gamma} + \text{h.c.}), \\
\hat{\mathbf{E}}(\mathbf{r}, t) &= -\frac{\partial \hat{\mathbf{A}}(\mathbf{r}, t)}{\partial t} = \sum_{\lambda_\gamma = \pm 1} \int \frac{d^3 k}{(2\pi)^3} i\omega (\mathbf{A}_{\mathbf{k}\lambda_\gamma}(\mathbf{r}, t) \hat{c}_{\mathbf{k}\lambda_\gamma} - \text{h.c.}), \\
\hat{\mathbf{H}}(\mathbf{r}, t) &= \nabla \times \hat{\mathbf{A}}(\mathbf{r}, t) = \sum_{\lambda_\gamma = \pm 1} \int \frac{d^3 k}{(2\pi)^3} i\mathbf{k} \times (\mathbf{A}_{\mathbf{k}\lambda_\gamma}(\mathbf{r}, t) \hat{c}_{\mathbf{k}\lambda_\gamma} - \text{h.c.})
\end{aligned} \tag{6}$$

where $\hat{c}_{\mathbf{k}\lambda_\gamma}$ are the annihilation operators and

$$\mathbf{A}_{\mathbf{k}\lambda_\gamma}(\mathbf{r}, t) = \frac{\sqrt{4\pi}}{\sqrt{2\omega}} \mathbf{e}_{\mathbf{k}\lambda_\gamma} e^{-i\omega t + i\mathbf{k}\cdot\mathbf{r}}, \tag{7}$$

where $\mathbf{e}_{\mathbf{k}\lambda_\gamma} \cdot \mathbf{k} = 0$, $\mathbf{e}_{\mathbf{k}\lambda_\gamma} \cdot \mathbf{e}_{\mathbf{k}'\lambda'_\gamma}^* = \delta_{\lambda_\gamma \lambda'_\gamma}$. Let us also define the following averages (cf. [3]):

$$\begin{aligned}
\langle 0 | \hat{\mathbf{A}}(\mathbf{r}, t) | \gamma \rangle &= \sum_{\lambda_\gamma} \int \frac{d^3 k}{(2\pi)^3} \mathbf{A}_{\mathbf{k}\lambda_\gamma}(\mathbf{r}, t) S_{fi}^{(1)}(\mathbf{k}, \lambda_\gamma), \\
\langle 0 | \hat{\mathbf{E}}(\mathbf{r}, t) | \gamma \rangle &= \sum_{\lambda_\gamma} \int \frac{d^3 k}{(2\pi)^3} i\omega \mathbf{A}_{\mathbf{k}\lambda_\gamma}(\mathbf{r}, t) S_{fi}^{(1)}(\mathbf{k}, \lambda_\gamma), \\
\langle 0 | \hat{\mathbf{H}}(\mathbf{r}, t) | \gamma \rangle &= \sum_{\lambda_\gamma} \int \frac{d^3 k}{(2\pi)^3} i[\mathbf{k} \times \mathbf{A}_{\mathbf{k}\lambda_\gamma}(\mathbf{r}, t)] S_{fi}^{(1)}(\mathbf{k}, \lambda_\gamma).
\end{aligned} \tag{8}$$

The diagonal part $\hat{S} - \hat{S}^{(1)} = \hat{\mathbf{1}}$ does not contribute to Eq.(8).

A spatial observable in this problem is *the energy density*, an electric part of which is

$$\begin{aligned}
\langle \gamma | \hat{\mathbf{E}}^2(\mathbf{r}, t) | \gamma \rangle &= \langle \gamma | \gamma \rangle \sum_{\lambda_\gamma} \int \frac{d^3 k}{(2\pi)^3} \omega^2 |\mathbf{A}_{\mathbf{k}\lambda_\gamma}(\mathbf{r}, t)|^2 + \\
+ 2 \sum_{\lambda_\gamma, \lambda'_\gamma} \int \frac{d^3 k}{(2\pi)^3} \frac{d^3 k'}{(2\pi)^3} \omega \omega' \mathbf{A}_{\mathbf{k}\lambda_\gamma}(\mathbf{r}, t) \cdot \mathbf{A}_{\mathbf{k}'\lambda'_\gamma}^*(\mathbf{r}, t) S_{fi}^{(1)}(\mathbf{k}, \lambda_\gamma) \left(S_{fi}^{(1)}(\mathbf{k}', \lambda'_\gamma) \right)^*
\end{aligned} \tag{9}$$

where $|\mathbf{A}_{\mathbf{k}\lambda_\gamma}(\mathbf{r}, t)|^2 = 2\pi/\omega$, so the first term

$$\varepsilon_0 = \langle \gamma | \gamma \rangle \sum_{\lambda_\gamma} \int \frac{d^3 k}{(2\pi)^3} \omega^2 |\mathbf{A}_{\mathbf{k}\lambda_\gamma}(\mathbf{r}, t)|^2 = \langle \gamma | \gamma \rangle \sum_{\lambda_\gamma} \int \frac{d^3 k}{(2\pi)^3} 2\pi\omega \tag{10}$$

diverges and should be associated with the vacuum energy. The diagonal term $\hat{S} - \hat{S}^{(1)} = \hat{\mathbf{1}}$ only contributes to the factor $\langle \gamma | \gamma \rangle$. The finite contribution is

$$\langle \gamma | \hat{\mathbf{E}}^2(\mathbf{r}, t) | \gamma \rangle - \varepsilon_0 = 2 \left| \langle 0 | \hat{\mathbf{E}}(\mathbf{r}, t) | \gamma \rangle \right|^2. \tag{11}$$

The magnetic counterpart looks as follows:

$$\begin{aligned}
\langle \gamma | \hat{\mathbf{H}}^2(\mathbf{r}, t) | \gamma \rangle &= \langle \gamma | \gamma \rangle \sum_{\lambda_\gamma} \int \frac{d^3 k}{(2\pi)^3} \mathbf{k}^2 |\mathbf{A}_{\mathbf{k}\lambda_\gamma}(\mathbf{r}, t)|^2 + \\
+ 2 \sum_{\lambda_\gamma, \lambda'_\gamma} \int \frac{d^3 k}{(2\pi)^3} \frac{d^3 k'}{(2\pi)^3} [\mathbf{k} \times \mathbf{A}_{\mathbf{k}\lambda_\gamma}(\mathbf{r}, t)] \cdot [\mathbf{k}' \times \mathbf{A}_{\mathbf{k}'\lambda'_\gamma}^*(\mathbf{r}, t)] S_{fi}^{(1)}(\mathbf{k}, \lambda_\gamma) \left(S_{fi}^{(1)}(\mathbf{k}', \lambda'_\gamma) \right)^* = \\
= \varepsilon_0 + 2 \left| \langle 0 | \hat{\mathbf{H}}(\mathbf{r}, t) | \gamma \rangle \right|^2.
\end{aligned} \tag{12}$$

Thus, a finite part of the spatial energy density is obtained as

$$\mathcal{W}(\mathbf{r}, t) = \frac{1}{8\pi} \langle \gamma | \hat{\mathbf{E}}^2(\mathbf{r}, t) + \hat{\mathbf{H}}^2(\mathbf{r}, t) | \gamma \rangle - \frac{\varepsilon_0}{4\pi} = \frac{1}{4\pi} \left(\left| \langle 0 | \hat{\mathbf{E}}(\mathbf{r}, t) | \gamma \rangle \right|^2 + \left| \langle 0 | \hat{\mathbf{H}}(\mathbf{r}, t) | \gamma \rangle \right|^2 \right), \quad (13)$$

and it can be interpreted as a probability to detect the emitted photon in a region of space-time centered at the point (\mathbf{r}, t) , whereas the electron is jointly detected as a plane wave with the quantum numbers \mathbf{p}', λ' .

Now as a next step we rewrite the electric part as follows:

$$\begin{aligned} \frac{1}{4\pi} \left| \langle 0 | \hat{\mathbf{E}}(\mathbf{r}, t) | \gamma \rangle \right|^2 &= \frac{1}{4\pi} \left| \sum_{\lambda_\gamma} \int \frac{d^3 k}{(2\pi)^3} \mathbf{E}_{\lambda_\gamma}(\mathbf{k}) e^{-i\mathbf{k} \cdot \mathbf{r}} \right|^2 = \\ &= \frac{1}{4\pi} \sum_{\lambda_\gamma, \tilde{\lambda}_\gamma} \int \frac{d^3 k}{(2\pi)^3} \frac{d^3 \tilde{k}}{(2\pi)^3} \mathbf{E}_{\lambda_\gamma}^*(\mathbf{k} - \tilde{\mathbf{k}}/2) \cdot \mathbf{E}_{\tilde{\lambda}_\gamma}(\mathbf{k} + \tilde{\mathbf{k}}/2) e^{-it(\omega(\mathbf{k}+\tilde{\mathbf{k}}/2) - \omega(\mathbf{k}-\tilde{\mathbf{k}}/2)) + i\mathbf{r} \cdot \tilde{\mathbf{k}}} \equiv \\ &\equiv \int \frac{d^3 k}{(2\pi)^3} \mathcal{W}(\mathbf{r}, \mathbf{k}, t), \end{aligned} \quad (14)$$

where

$$\mathbf{E}_{\lambda_\gamma}(\mathbf{k}) = \frac{i\omega\sqrt{4\pi}}{\sqrt{2\omega n^2}} e_{\mathbf{k}\lambda_\gamma} \sum_{\lambda} \int \frac{d^3 p}{(2\pi)^3} f_e^{(\text{in})}(\mathbf{p}, \lambda) S_{fi}^{(1)}(\mathbf{p}, \lambda, \mathbf{k}, \lambda_\gamma) \quad (15)$$

is a positive-frequency component of the electric field of the evolved state from Eq.(8) and

$$\mathcal{W}(\mathbf{r}, \mathbf{k}, t) = \frac{1}{4\pi} \sum_{\lambda_\gamma, \tilde{\lambda}_\gamma} \int \frac{d^3 \tilde{k}}{(2\pi)^3} \mathbf{E}_{\lambda_\gamma}^*(\mathbf{k} - \tilde{\mathbf{k}}/2) \cdot \mathbf{E}_{\tilde{\lambda}_\gamma}(\mathbf{k} + \tilde{\mathbf{k}}/2) e^{-it(\omega(\mathbf{k}+\tilde{\mathbf{k}}/2) - \omega(\mathbf{k}-\tilde{\mathbf{k}}/2)) + i\mathbf{r} \cdot \tilde{\mathbf{k}}}, \quad (16)$$

is a Wigner function of the photon evolved state in phase space (see, for instance, [4]). Here $f_e^{(\text{in})}(\mathbf{p}, \lambda)$ is the wave function of the incoming electron from Eq.(5), and we have used the normalization of the photon potential in a transparent medium with a refractive index $n(\omega) > 1$, see [5].

Eq.(14) shows that one marginal distribution of this Wigner function yields the energy density of the photon field in real space and time. The other marginal distribution (the connection between the matrices S_{fi} , T_{fi} , and M_{fi} is given in [1, 2])

$$\begin{aligned} \int d^3 x \mathcal{W}(\mathbf{r}, \mathbf{k}, t) &= \frac{\omega}{2n^2} \left| \sum_{\lambda} \int \frac{d^3 p}{(2\pi)^3} f_e^{(\text{in})}(\mathbf{p}, \lambda) S_{fi}(\mathbf{p}, \lambda, \mathbf{k}, \lambda_\gamma) \right|^2 = \\ &= \frac{\omega}{2n^2} (2\pi)^2 \frac{T}{2\pi} \delta(\varepsilon(\mathbf{p}) - \varepsilon'(\mathbf{p}') - \omega(\mathbf{k})) \frac{4\pi}{2\omega(\mathbf{k})n^2(\omega(\mathbf{k}))2\varepsilon(\mathbf{p})2\varepsilon'(\mathbf{p}')} \left| \sum_{\lambda} f_e^{(\text{in})}(\mathbf{p}, \lambda) M_{fi}(\mathbf{p}, \mathbf{k}, \lambda, \lambda_\gamma) \right|_{\mathbf{p}=\mathbf{p}'+\mathbf{k}}^2 \end{aligned} \quad (17)$$

yields probability to detect the photon with the frequency ω and the wave vector \mathbf{k} (here $T \rightarrow \infty$ is a very long period of time [1, 2]), that is, the result of the quantum theory of ChR in momentum space [5]. It does *not* depends on a phase of the complex amplitude M_{fi} , even if the incoming electron is a wave packet. When the latter is a plane wave with the momentum $\langle \mathbf{p} \rangle$ and the helicity λ_e , we have $f_e^{(\text{in})}(\mathbf{p}, \lambda) \rightarrow \text{const } \delta_{\lambda\lambda_e} \delta(\mathbf{p} - \langle \mathbf{p} \rangle)$ and Eq.(17) reproduces the standard probability of the plane-wave approximation,

$$\int d^3 x \mathcal{W}(\mathbf{r}, \mathbf{k}, t) \propto |S_{fi}(\langle \mathbf{p} \rangle, \lambda_e, \mathbf{k}, \lambda_\gamma)|^2. \quad (18)$$

To understand what new information – compared to the momentum space – the Wigner function in phase space and the marginal distribution (14) bring about, we write the complex amplitude as

$$M_{fi}(\mathbf{p}, \mathbf{k}, \lambda_e, \lambda_\gamma) = |M_{fi}(\mathbf{p}, \mathbf{k}, \lambda_e, \lambda_\gamma)| \exp \{ i\zeta_{fi}(\mathbf{p}, \mathbf{k}, \lambda_e, \lambda_\gamma) \} \quad (19)$$

where $\zeta_{fi}(\mathbf{p}, \mathbf{k}, \lambda_e, \lambda_\gamma)$ is a dynamic phase (see, for instance, [6–8]). Importantly, this phase *is non-vanishing* even at the tree level – see Sec.5. The Wigner function of the photon field in phase space is defined by the following *master integral* $\mathcal{W}_p(\mathbf{r}, \mathbf{p}, \mathbf{k}, t)$:

$$\begin{aligned} \mathcal{W}(\mathbf{r}, \mathbf{k}, t) &= (2\pi)^5 \sum_{\lambda_\gamma, \tilde{\lambda}_\gamma} \sum_{\lambda \tilde{\lambda}} \int \frac{d^3 p}{(2\pi)^3} \delta(\mathbf{p} - \mathbf{p}' - \mathbf{k}) \int \frac{d^3 \tilde{k}}{(2\pi)^3} \sqrt{\frac{\omega(\mathbf{k} + \tilde{\mathbf{k}}/2)\omega(\mathbf{k} - \tilde{\mathbf{k}}/2)}{2n^2(\omega(\mathbf{k} + \tilde{\mathbf{k}}/2))2n^2(\omega(\mathbf{k} - \tilde{\mathbf{k}}/2))}} \\ &\times \mathbf{e}_{\mathbf{k} - \tilde{\mathbf{k}}/2, \tilde{\lambda}_\gamma}^* \cdot \mathbf{e}_{\mathbf{k} + \tilde{\mathbf{k}}/2, \lambda_\gamma} \left(f_e^{(\text{in})}(\mathbf{p} - \tilde{\mathbf{k}}/2, \tilde{\lambda}) \right)^* f_e^{(\text{in})}(\mathbf{p} + \tilde{\mathbf{k}}/2, \lambda) \delta\left(\varepsilon(\mathbf{p} + \tilde{\mathbf{k}}/2) - \varepsilon' - \omega(\mathbf{k} + \tilde{\mathbf{k}}/2)\right) \\ &\times \delta\left(\varepsilon(\mathbf{p} - \tilde{\mathbf{k}}/2) - \varepsilon' - \omega(\mathbf{k} - \tilde{\mathbf{k}}/2)\right) T_{fi}\left(\mathbf{p} + \tilde{\mathbf{k}}/2, \lambda, \mathbf{k} + \tilde{\mathbf{k}}/2, \lambda_\gamma\right) T_{fi}^*\left(\mathbf{p} - \tilde{\mathbf{k}}/2, \tilde{\lambda}, \mathbf{k} - \tilde{\mathbf{k}}/2, \tilde{\lambda}_\gamma\right) \\ &\times e^{-it(\omega(\mathbf{k} + \tilde{\mathbf{k}}/2) - \omega(\mathbf{k} - \tilde{\mathbf{k}}/2)) + i\mathbf{r} \cdot \tilde{\mathbf{k}}} \equiv \\ &\equiv \int \frac{d^3 p}{(2\pi)^3} (2\pi)^3 \delta(\mathbf{p} - \mathbf{p}' - \mathbf{k}) \mathcal{W}_p(\mathbf{r}, \mathbf{p}, \mathbf{k}, t) = \mathcal{W}_p(\mathbf{r}, \mathbf{p} = \mathbf{p}' + \mathbf{k}, \mathbf{k}, t), \end{aligned} \quad (20)$$

so that $\mathcal{W}(\mathbf{r}, \mathbf{k}, t) = \mathcal{W}_p(\mathbf{r}, \mathbf{p} = \mathbf{p}' + \mathbf{k}, \mathbf{k}, t)$. Note that no approximations have been made so far. The product

$$\begin{aligned} &f_e^{(\text{in})}(\mathbf{p} + \tilde{\mathbf{k}}/2, \lambda) \left(f_e^{(\text{in})}(\mathbf{p} - \tilde{\mathbf{k}}/2, \tilde{\lambda}) \right)^* = \\ &= \delta_{\lambda, \lambda_e} \delta_{\tilde{\lambda}, \lambda_e} \left(\frac{2\sqrt{\pi}}{\sigma} \right)^3 \exp \left\{ -\frac{(\mathbf{p} - \langle \mathbf{p} \rangle)^2}{\sigma^2} - \left(\frac{\tilde{\mathbf{k}}}{2\sigma} \right)^2 \right\} \end{aligned} \quad (21)$$

is also Gaussian.

If the final electron is *not measured*, which is often the case for ChR, the spatio-temporal distribution of the emitted energy is obtained by tracing out the electron quantum numbers,

$$\begin{aligned} \sum_{\lambda'} \int \frac{d^3 p'}{(2\pi)^3} \frac{1}{4\pi} \left| \langle 0 | \hat{\mathbf{E}}(\mathbf{r}, t) | \gamma \rangle \right|^2 &= \sum_{\lambda'} \int \frac{d^3 p'}{(2\pi)^3} \frac{d^3 k}{(2\pi)^3} \mathcal{W}(\mathbf{r}, \mathbf{k}, t) = \\ &= \sum_{\lambda'} \int \frac{d^3 p}{(2\pi)^3} \frac{d^3 k}{(2\pi)^3} \mathcal{W}_p(\mathbf{r}, \mathbf{p}, \mathbf{k}, t) \Big|_{\mathbf{p}' = \mathbf{p} - \mathbf{k}}. \end{aligned} \quad (22)$$

Thus, by using the phase space formalism, one can trace the dynamics of the photon field formation, spreading, and interference in real space and time, which is unattainable even in the fully quantum theory in momentum space. Moreover, this intrinsic dynamics turns out to be closely tied to the coherence length of the electron packet and to the phase ζ_{fi} of the amplitude. Analogously to quantum optics [4], we deal with two marginal distributions, complementary to each other, only one of which is commonly used in the photon emission analysis.

3 Paraxial Wigner function

In calculating the integral over $\tilde{\mathbf{k}}$ in Eq.(20), we make the paraxial approximation in which $\sigma \ll m$ and we neglect the terms $\mathcal{O}(\tilde{\mathbf{k}})$ in the amplitude but keep those of $\mathcal{O}(\tilde{\mathbf{k}}^2)$ in the phase. The resultant integral over $\tilde{\mathbf{k}}$ is Gaussian. The calculations are very similar to those of the quasi-classical approximation in relativistic quantum mechanics [9] and there are regions in phase space – analogous to the well-known turning points – where this approximation fails to work. In practice, this region lies within very small emission angles, $\theta \sim \sigma/m < 10^{-3}$, which are of no practical interest for studies of ChR.

The linear \mathbf{k} -terms only come to the pre-exponential factor due to

$$\mathbf{e}_{\mathbf{k} - \tilde{\mathbf{k}}/2, \tilde{\lambda}_\gamma}^* \cdot \mathbf{e}_{\mathbf{k} + \tilde{\mathbf{k}}/2, \lambda_\gamma} = \delta_{\tilde{\lambda}_\gamma, \lambda_\gamma} + \frac{\tilde{k}_i}{2} \left(\mathbf{e}_{\mathbf{k}, \tilde{\lambda}_\gamma}^* \cdot \frac{\partial \mathbf{e}_{\mathbf{k}, \lambda_\gamma}}{\partial k_i} - \mathbf{e}_{\mathbf{k}, \lambda_\gamma} \cdot \frac{\partial \mathbf{e}_{\mathbf{k}, \tilde{\lambda}_\gamma}^*}{\partial k_i} \right) + \mathcal{O}(\tilde{k}^2) \quad (23)$$

The similar expansion of the amplitudes at $\tilde{\lambda}_\gamma = \lambda_\gamma, \tilde{\lambda} = \lambda = \lambda_e$ yields

$$\begin{aligned} &M_{fi}(\mathbf{p} + \tilde{\mathbf{k}}/2, \mathbf{k} + \tilde{\mathbf{k}}/2, \lambda_e, \lambda_\gamma) M_{fi}^*(\mathbf{p} - \tilde{\mathbf{k}}/2, \mathbf{k} - \tilde{\mathbf{k}}/2, \lambda_e, \lambda_\gamma) = \\ &\left(|M_{fi}(\mathbf{p}, \mathbf{k}, \lambda_e, \lambda_\gamma)|^2 + \mathcal{O}(\tilde{\mathbf{k}}^2) \right) \exp \left\{ i\tilde{\mathbf{k}} \cdot (\partial_{\mathbf{p}} + \partial_{\mathbf{k}}) \zeta_{fi}(\mathbf{p}, \mathbf{k}, \lambda_e, \lambda_\gamma) + \mathcal{O}(\tilde{\mathbf{k}}^3) \right\}. \end{aligned} \quad (24)$$

Neglecting the linear correction in Eq.(23), we need to calculate the following master integral:

$$\begin{aligned} \mathcal{W}_p(\mathbf{r}, \mathbf{p}, \mathbf{k}, t) &= (2\pi)^2 \sqrt{4\pi} \sum_{\lambda_\gamma} \frac{|M_{fi}(\mathbf{p}, \lambda_e, \mathbf{k}, \lambda_\gamma)|^2}{(2n^2(\mathbf{k}))^2 2\varepsilon' 2\varepsilon(\mathbf{p})} \int \frac{d^3 \tilde{\mathbf{k}}}{(2\pi)^3} \frac{dt'}{2\pi} \frac{d\tau}{2\pi} \left(f_e^{(\text{in})}(\mathbf{p} - \tilde{\mathbf{k}}/2) \right)^* f_e^{(\text{in})}(\mathbf{p} + \tilde{\mathbf{k}}/2) \\ &\times \exp \left\{ it'(\varepsilon(\mathbf{p}) - \varepsilon' - \omega(\mathbf{k})) + i\tilde{\mathbf{k}} \cdot (\mathbf{r} - \mathbf{u}_p t + (\partial_{\mathbf{p}} + \partial_{\mathbf{k}})\zeta_{fi} + \tau(\mathbf{u}_p - \mathbf{u}_k)) + it' \frac{1}{2} \frac{\tilde{k}_i \tilde{k}_j}{2} (\partial_{ij}^2 \varepsilon - \partial_{ij}^2 \omega) \right\} \end{aligned} \quad (25)$$

where we have taken the equality $\tilde{\mathbf{k}} \cdot \mathbf{u}_p = \tilde{\mathbf{k}} \cdot \mathbf{u}_k$ into account, which holds within the paraxial approximation. Here

$$\begin{aligned} \mathbf{u}_p &= \frac{\partial \varepsilon(\mathbf{p})}{\partial \mathbf{p}} = \frac{\mathbf{p}}{\varepsilon(\mathbf{p})}, \quad \varepsilon(\mathbf{p}) = \sqrt{m^2 + \mathbf{p}^2}, \quad \mathbf{u}_k = \frac{\partial \omega(\mathbf{k})}{\partial \mathbf{k}}, \\ \partial_{ij}^2 \varepsilon(\mathbf{p}) &\equiv \frac{\partial^2 \varepsilon(\mathbf{p})}{\partial p_i \partial p_j} = \frac{1}{\varepsilon(\mathbf{p})} (\delta_{ij} - (\mathbf{u}_p)_i (\mathbf{u}_p)_j). \end{aligned} \quad (26)$$

We take a medium with *weak dispersion* from now on, for which

$$\frac{\omega}{n(\omega)} \frac{dn(\omega)}{d\omega} \ll 1, \quad (27)$$

and we find (recall that $\mathbf{k}^2 = n^2(\omega)\omega^2$)

$$\begin{aligned} \mathbf{u}_k &= \frac{\partial \omega}{\partial \mathbf{k}} \approx \frac{\mathbf{k}}{n^2 \omega} = \frac{\mathbf{k}/|\mathbf{k}|}{n}, \\ \partial_{ij}^2 \omega &\equiv \frac{\partial^2 \omega}{\partial k_i \partial k_j} \approx \frac{1}{n^2 \omega} \left(\delta_{ij} - \frac{k_i k_j}{\mathbf{k}^2} \right). \end{aligned} \quad (28)$$

Clearly, the photon group velocity in the medium, $|\mathbf{u}_k| = 1/n < 1$ as $n > 1$.

Taking the incoming packet from Eq.(5), we get

$$\begin{aligned} \mathcal{W}_p(\mathbf{r}, \mathbf{p}, \mathbf{k}, t) &= (2\pi)^2 \sqrt{4\pi} \sum_{\lambda_\gamma} \left(\frac{2\sqrt{\pi}}{\sigma} \right)^3 \frac{|M_{fi}(\mathbf{p}, \lambda_e, \mathbf{k}, \lambda_\gamma)|^2}{(2n^2(\mathbf{k}))^2 2\varepsilon' 2\varepsilon(\mathbf{p})} \exp \left\{ -\frac{(\mathbf{p} - \langle \mathbf{p} \rangle)^2}{\sigma^2} \right\} \\ &\times \int \frac{d^3 \tilde{\mathbf{k}}}{(2\pi)^3} \frac{dt'}{2\pi} \frac{d\tau}{2\pi} \exp \left\{ it'(\varepsilon(\mathbf{p}) - \varepsilon' - \omega(\mathbf{k})) - \mathcal{A} \cdot \tilde{\mathbf{k}} - \frac{1}{2} \tilde{k}_i \tilde{k}_j B_{ij} \right\}, \end{aligned} \quad (29)$$

where we find

$$\begin{aligned} \mathcal{A}(t, \tau) &= -i \left(\mathbf{r} - \mathbf{u}_p t + (\partial_{\mathbf{p}} + \partial_{\mathbf{k}})\zeta_{fi} + \tau(\mathbf{u}_p - \mathbf{u}_k) \right), \\ B_{ij}(t') &= \delta_{ij} \frac{1}{2\sigma^2} - \frac{it'}{4} (\partial_{ij}^2 \varepsilon - \partial_{ij}^2 \omega) \approx \delta_{ij} \left(\frac{1}{2\sigma^2} + \frac{it'}{4} \left(\frac{1}{\omega n^2} - \frac{1}{\varepsilon} \right) \right) + \frac{it'}{4} \left(\frac{1}{\varepsilon} - \frac{1}{\omega} \right) (\mathbf{u}_p)_i (\mathbf{u}_p)_j. \end{aligned} \quad (30)$$

We evaluate the Gaussian integral as

$$\int \frac{d^3 \tilde{\mathbf{k}}}{(2\pi)^3} \exp \left\{ -\mathcal{A} \cdot \tilde{\mathbf{k}} - \frac{1}{2} \tilde{k}_i \tilde{k}_j B_{ij} \right\} = (2\pi)^{-3/2} \frac{1}{\sqrt{\det B}} \exp \left\{ \frac{1}{2} B_{ij}^{-1} \mathcal{A}_i \mathcal{A}_j \right\}, \quad (31)$$

where

$$\begin{aligned} \det B &= \eta^2 (\eta + \chi \mathbf{u}_p^2), \quad B_{ij}^{-1} = \eta^{-1} \delta_{ij} - \frac{\chi}{\eta(\eta + \chi \mathbf{u}_p^2)} (\mathbf{u}_p)_i (\mathbf{u}_p)_j, \\ \eta(t') &= \frac{1}{2\sigma^2} + \frac{it'}{4} \left(\frac{1}{\omega n^2} - \frac{1}{\varepsilon} \right), \quad \chi(t') = \frac{it'}{4} \left(\frac{1}{\varepsilon} - \frac{1}{\omega} \right). \end{aligned} \quad (32)$$

The integral over τ is also Gaussian and evaluated as follows:

$$\int_{-\infty}^{+\infty} \frac{d\tau}{2\pi} \exp \left\{ \frac{1}{2} B_{ij}^{-1} \mathcal{A}_i \mathcal{A}_j \right\} = \frac{1}{\sqrt{2\pi}} \sqrt{\frac{\eta + \chi \mathbf{u}_p^2}{(\mathbf{u}_p - \mathbf{u}_k)^2 + \frac{\chi}{\eta} [\mathbf{u}_p \times \mathbf{u}_k]^2}}$$

$$\times \exp \left\{ -\frac{1}{2\eta} \frac{[\mathbf{R} \times (\mathbf{u}_p - \mathbf{u}_k)]^2 + \frac{\chi}{\eta} (\mathbf{u}_p \cdot [\mathbf{R} \times \mathbf{u}_k])^2}{(\mathbf{u}_p - \mathbf{u}_k)^2 + \frac{\chi}{\eta} [\mathbf{u}_p \times \mathbf{u}_k]^2} \right\}, \quad (33)$$

where

$$\begin{aligned} \mathbf{R} &= \mathbf{r} - \mathbf{u}_p t + (\partial_{\mathbf{p}} + \partial_{\mathbf{k}}) \zeta_{fi}(\mathbf{p}, \lambda_e, \mathbf{k}, \lambda_\gamma) \equiv \\ &\equiv \{X, Y, Z\} = R \{\sin \theta_R \cos \phi_R, \sin \theta_R \sin \phi_R, \cos \theta_R\}. \end{aligned} \quad (34)$$

We can rewrite the pre-exponential factor as follows:

$$\begin{aligned} \sqrt{\frac{\eta + \chi \mathbf{u}_p^2}{\det B \left((\mathbf{u}_p - \mathbf{u}_k)^2 + \frac{\chi}{\eta} [\mathbf{u}_p \times \mathbf{u}_k]^2 \right)}} &= \sqrt{\frac{1}{\eta (\eta (\mathbf{u}_p - \mathbf{u}_k)^2 + \chi [\mathbf{u}_p \times \mathbf{u}_k]^2)}} \equiv \frac{1}{G(t')} \exp \left\{ -\frac{i}{2} g(t') \right\}, \\ G(t') &= \left[\left(\frac{1}{(2\sigma^2)^2} + \left(\frac{t'}{4} \right)^2 \left(\frac{1}{\omega n^2} - \frac{1}{\varepsilon} \right)^2 \right) \right. \\ &\quad \left. \times \left(\frac{(\mathbf{u}_p - \mathbf{u}_k)^4}{(2\sigma^2)^2} + \left(\frac{t'}{4} \right)^2 \left(\left(\frac{1}{\omega n^2} - \frac{1}{\varepsilon} \right) (\mathbf{u}_p - \mathbf{u}_k)^2 + \left(\frac{1}{\varepsilon} - \frac{1}{\omega} \right) [\mathbf{u}_p \times \mathbf{u}_k]^2 \right)^2 \right) \right]^{1/4}, \\ g(t') &= \arctan \frac{t'}{8\sigma^2 \frac{(\mathbf{u}_p - \mathbf{u}_k)^2}{(2\sigma^2)^2} - \left(\frac{t'}{4} \right)^2 \left(\frac{1}{\omega n^2} - \frac{1}{\varepsilon} \right) \left(\left(\frac{1}{\omega n^2} - \frac{1}{\varepsilon} \right) (\mathbf{u}_p - \mathbf{u}_k)^2 + \left(\frac{1}{\varepsilon} - \frac{1}{\omega} \right) [\mathbf{u}_p \times \mathbf{u}_k]^2 \right)}. \end{aligned} \quad (35)$$

One can alternatively represent the l.h.s of Eq.(35) in terms of two Gouy phases as follows:

$$g(t') = g_1(t') + g_2(t') \quad (36)$$

where

$$\begin{aligned} g_1(t') &= \arctan \frac{t'}{t_d}, \quad t_d = \frac{2}{\sigma^2} \frac{(\mathbf{u}_p - \mathbf{u}_k)^2}{\left(\frac{1}{\omega n^2} - \frac{1}{\varepsilon} \right) (\mathbf{u}_p - \mathbf{u}_k)^2 + \left(\frac{1}{\varepsilon} - \frac{1}{\omega} \right) [\mathbf{u}_p \times \mathbf{u}_k]^2}, \\ g_2(t') &= \arctan \frac{t'}{\tilde{t}_d}, \quad \tilde{t}_d = \frac{2}{\sigma^2} \frac{1}{\frac{1}{\omega n^2} - \frac{1}{\varepsilon}} = \frac{2}{\sigma^2} \frac{\omega n^2}{1 - n^2 \omega / \varepsilon}. \end{aligned} \quad (37)$$

Note that $\tilde{t}_d = t_d(\theta = 0)$ where the photon emission angle θ is counted from the electron partial momentum \mathbf{p} . Therefore

$$\begin{aligned} G(t') &= \frac{|\mathbf{u}_p - \mathbf{u}_k|}{2\sigma^2} \left[(1 + (t'/t_d)^2) (1 + (t'/\tilde{t}_d)^2) \right]^{1/4}, \\ \sqrt{\frac{\eta + \chi \mathbf{u}_p^2}{\det B \left((\mathbf{u}_p - \mathbf{u}_k)^2 + \frac{\chi}{\eta} [\mathbf{u}_p \times \mathbf{u}_k]^2 \right)}} &= \frac{2\sigma^2}{|\mathbf{u}_p - \mathbf{u}_k| \left[(1 + (t'/t_d)^2) (1 + (t'/\tilde{t}_d)^2) \right]^{1/4}} \\ &\quad \times \exp \left\{ -\frac{i}{2} \left(\arctan \frac{t'}{t_d} + \arctan \frac{t'}{\tilde{t}_d} \right) \right\}. \end{aligned} \quad (38)$$

So the master integral within the paraxial approximation becomes

$$\begin{aligned} \mathcal{W}_p(\mathbf{r}, \mathbf{p}, \mathbf{k}, t) &= \left(\frac{2\sqrt{\pi}}{\sigma} \right)^3 \frac{\sqrt{4\pi}}{(2n^2(\mathbf{k}))^2 2\varepsilon' 2\varepsilon(\mathbf{p})} \sum_{\lambda_\gamma} |M_{fi}(\mathbf{p}, \lambda_e, \mathbf{k}, \lambda_\gamma)|^2 \exp \left\{ -\frac{(\mathbf{p} - \langle \mathbf{p} \rangle)^2}{\sigma^2} \right\} \\ &\quad \times \int_{-\infty}^{+\infty} \frac{dt'}{2\pi} \frac{1}{G(t')} \exp \left\{ it'(\varepsilon(\mathbf{p}) - \varepsilon' - \omega(\mathbf{k})) - \frac{i}{2} g(t') - \right. \\ &\quad \left. - \frac{1}{2\eta(t')} \frac{\eta(t') [\mathbf{R} \times (\mathbf{u}_p - \mathbf{u}_k)]^2 + \chi(t') (\mathbf{R} \cdot [\mathbf{u}_p \times \mathbf{u}_k])^2}{\eta(t') (\mathbf{u}_p - \mathbf{u}_k)^2 + \chi(t') [\mathbf{u}_p \times \mathbf{u}_k]^2} \right\}. \end{aligned} \quad (39)$$

This expression is not applicable at the very small angles $\theta \lesssim \sigma/m \ll 1$ where σ/m is usually smaller than 10^{-3} meaning that the spatial coherence length of the electron packet $\sigma_x = 1/\sigma$ is larger than a few angstroms.

The exponent in Eq.(39) can be presented as follows:

$$\begin{aligned}
& -\frac{1}{2\eta(t')} \frac{\eta(t')[\mathbf{R} \times (\mathbf{u}_p - \mathbf{u}_k)]^2 + \chi(t')(\mathbf{R} \cdot [\mathbf{u}_p \times \mathbf{u}_k])^2}{\eta(t')(\mathbf{u}_p - \mathbf{u}_k)^2 + \chi(t')[\mathbf{u}_p \times \mathbf{u}_k]^2} = \\
& = -\sigma^2 \frac{1 - it'/\tilde{t}_d}{1 + (t'/\tilde{t}_d)^2} \frac{1 - it'/t_d}{1 + (t'/t_d)^2} \left(\frac{[\mathbf{R} \times (\mathbf{u}_p - \mathbf{u}_k)]^2}{(\mathbf{u}_p - \mathbf{u}_k)^2} \left(1 + \frac{it'}{\tilde{t}_d}\right) + it' \frac{\sigma^2}{2} \left(\frac{1}{\varepsilon} - \frac{1}{\omega}\right) \frac{(\mathbf{R} \cdot [\mathbf{u}_p \times \mathbf{u}_k])^2}{(\mathbf{u}_p - \mathbf{u}_k)^2} \right) \quad (40)
\end{aligned}$$

The real part of this is

$$\begin{aligned}
\text{Re}(40) & = -\frac{1}{\sigma_x^2(t')} \left(\underbrace{\frac{[\mathbf{R} \times (\mathbf{u}_p - \mathbf{u}_k)]^2}{(\mathbf{u}_p - \mathbf{u}_k)^2}}_{\text{finite at } t' = 0} + \underbrace{\frac{(t')^2}{\tau_d^2(1 + (t'/\tilde{t}_d)^2)} \frac{(\mathbf{R} \cdot [\mathbf{u}_p \times \mathbf{u}_k])^2}{(\mathbf{u}_p - \mathbf{u}_k)^2}}_{\text{due to spreading at } t' \neq 0} \right) \equiv -\frac{R^2}{R_{\text{eff}}^2(t')}, \\
\sigma_x^2(t') & = \sigma^{-2} (1 + (t'/t_d)^2), \quad \tau_d^2 = \frac{2}{\sigma^2} \frac{t_d \tilde{t}_d}{\left(\frac{1}{\varepsilon} - \frac{1}{\omega}\right) (t_d + \tilde{t}_d)}, \quad (41)
\end{aligned}$$

The imaginary part

$$\text{Im}(40) = \frac{t'}{\sigma^2(t')} \left(\frac{1}{t_d} \frac{[\mathbf{R} \times (\mathbf{u}_p - \mathbf{u}_k)]^2}{(\mathbf{u}_p - \mathbf{u}_k)^2} - \frac{\sigma^2}{2} \left(\frac{1}{\varepsilon} - \frac{1}{\omega}\right) \frac{1 - t'^2/(t_d \tilde{t}_d)}{1 + t'^2/\tilde{t}_d^2} \frac{(\mathbf{R} \cdot [\mathbf{u}_p \times \mathbf{u}_k])^2}{(\mathbf{u}_p - \mathbf{u}_k)^2} \right) \quad (42)$$

vanishes at $t' = 0$. And so

$$\begin{aligned}
& \int_{-\infty}^{+\infty} \frac{dt'}{2\pi} \frac{1}{G(t')} \exp \left\{ it'(\varepsilon(\mathbf{p}) - \varepsilon' - \omega(\mathbf{k})) - \frac{i}{2} g(t') - \frac{1}{2\eta(t')} \frac{\eta(t')[\mathbf{R} \times (\mathbf{u}_p - \mathbf{u}_k)]^2 + \chi(t')(\mathbf{R} \cdot [\mathbf{u}_p \times \mathbf{u}_k])^2}{\eta(t')(\mathbf{u}_p - \mathbf{u}_k)^2 + \chi(t')[\mathbf{u}_p \times \mathbf{u}_k]^2} \right\} = \\
& = 2 \int_0^{\infty} dt' \frac{e^{-R^2/R_{\text{eff}}^2(t')}}{G(t')} \cos \left(t'(\varepsilon(\mathbf{p}) - \varepsilon' - \omega(\mathbf{k})) - \frac{1}{2} g(t') + \text{Im}(40) \right), \quad (43)
\end{aligned}$$

which is why the master integral and the Wigner function are real but *not everywhere positive*. We employ this expression in the main part of the manuscript.

The paraxial Wigner function implies the momentum conservation law for every partial wave, $\mathbf{p} = \mathbf{p}' + \mathbf{k}$ where $|\mathbf{k}| = n\omega(\mathbf{k})$, but in the phase space there is *no* corresponding energy conservation for the partial waves, $\varepsilon(\mathbf{p}) - \varepsilon' - \omega(\mathbf{k}) \neq 0$, due to spreading and dependence of the integrand in Eq.(43) on t' . As a result, the well-known Cherenkov condition of the momentum space (see, e.g., [5]) does *not* hold within the formation or pre-wave zone,

$$\cos \theta \neq \cos \theta_{\text{Ch}} = \frac{1}{\beta n} + \frac{\omega}{2\varepsilon} \frac{n^2 - 1}{\beta n}, \quad (44)$$

which is why the photon field is *not* vanishing at the angles different from θ_{Ch} , a hallmark of the pre-wave zone [10, 11]. Likewise, there is no sharp spectral cutoff (see the debates in [5, 12])

$$\omega \not\ll \omega_{\text{cut-off}} = 2\varepsilon \frac{\beta n - 1}{n^2 - 1}, \quad (45)$$

even neglecting the dispersion of $n(\omega)$. One can see from Eq.(39) that the common features of the far-field Cherenkov radiation are regained when we neglect the spreading, that is, the dependence on time t' of the terms under the integral in Eq.(43). This can also be done when the incoming electron is a delocalized plane wave with $\sigma \rightarrow 0$ because the Gouy phase vanishes when either $t' \ll t_d$ or $\sigma \ll m$, and the limit of $G(t'), g(t')$ is the same in both these cases.

4 Transverse momentum conservation

When calculating the above Wigner function and the quantum shift of the photon arrival time, we employ the following representation of the delta function of the transverse momentum conservation in cylindrical coordinates:

$$\delta^{(2)}(\mathbf{p}_{\perp} - \mathbf{p}'_{\perp} - \mathbf{k}_{\perp}) =$$

$$\begin{aligned}
&= \frac{\Theta(p_\perp, k_\perp, p'_\perp)}{2\Delta} \left(\delta(\phi' - \phi + \alpha) \delta(\phi_\gamma - \phi - \gamma) + \delta(\phi' - \phi - \alpha) \delta(\phi_\gamma - \phi + \gamma) \right) = \\
&= \frac{\Theta(p_\perp, k_\perp, p'_\perp)}{2\Delta} \left(\delta(\phi' - \phi_\gamma - (\beta - \pi)) \delta(\phi_\gamma - \phi - \gamma) + \delta(\phi' - \phi_\gamma + (\beta - \pi)) \delta(\phi_\gamma - \phi + \gamma) \right), \quad (46)
\end{aligned}$$

where Δ is an area of a triangle with the legs $p_\perp, p'_\perp, k_\perp$ (see [13]) and the angles α, β, γ ($\alpha + \beta + \gamma = \pi$),

$$\begin{aligned}
\Delta &= \frac{1}{2} p_\perp p'_\perp \sin \alpha = \frac{1}{2} k_\perp p'_\perp \sin \beta = \frac{1}{2} p_\perp k_\perp \sin \gamma, \\
\alpha &= \arccos \left\{ \frac{p_\perp^2 + (p'_\perp)^2 - k_\perp^2}{2p_\perp p'_\perp} \right\}, \quad \beta = \arccos \left\{ \frac{(p'_\perp)^2 + k_\perp^2 - p_\perp^2}{2k_\perp p'_\perp} \right\}, \quad \gamma = \arccos \left\{ \frac{p_\perp^2 + k_\perp^2 - (p'_\perp)^2}{2k_\perp p_\perp} \right\} \quad (47)
\end{aligned}$$

and the legs satisfy the triangle rules,

$$p_\perp \leq k_\perp + p'_\perp, \quad p'_\perp \leq k_\perp + p_\perp, \quad k_\perp \leq p_\perp + p'_\perp. \quad (48)$$

The function $\Theta(p_\perp, k_\perp, p'_\perp)$ in Eq.(46) equals 1 when these inequalities are simultaneously satisfied and vanishes otherwise. Therefore

$$\frac{1}{2\Delta} = \frac{1}{k_\perp p'_\perp \sqrt{1 - \cos^2 \beta}} = \frac{2}{\sqrt{(k_\perp + p'_\perp - p_\perp)(k_\perp + p_\perp - p'_\perp)(p_\perp + p'_\perp - k_\perp)(k_\perp + p'_\perp + p_\perp)}}, \quad (49)$$

and the singularity at $k_\perp \rightarrow 0$ is integrable, i.e.

$$\int_0^\infty \frac{dk_\perp k_\perp}{2\Delta} \text{ is finite.} \quad (50)$$

The two momentum configurations from Eq.(46) yield different signs of the shift in the photon arrival time from the main manuscript, keeping the same absolute value – see Eq.(61) below.

5 Helicity amplitudes and the phase

The first-order amplitude of emission of a photon by an electron is

$$M_{fi} = \sqrt{4\pi\alpha} \bar{u}_{\mathbf{p}'\lambda'} \gamma^\mu e_\mu^* u_{\mathbf{p}\lambda} = |M_{fi}| e^{i\zeta_{fi}}, \quad (51)$$

where $\gamma^\mu e_\mu^* = -\boldsymbol{\gamma} \cdot \mathbf{e}_{\mathbf{k}\lambda_\gamma}^*$ in the Coulomb gauge, and each bispinor and vector are expanded in the following series:

$$\begin{aligned}
u_{\mathbf{p}\lambda} &= \sum_{\sigma=\pm 1/2} u_{\varepsilon\lambda}^{(\sigma)} d_{\sigma\lambda}^{(1/2)}(\theta) e^{-i\sigma\phi}, \\
\bar{u}_{\mathbf{p}'\lambda'} &= \sum_{\sigma'=\pm 1/2} \bar{u}_{\varepsilon'\lambda'}^{(\sigma')} d_{\sigma'\lambda'}^{(1/2)}(\theta') e^{i\sigma'\phi'}, \\
\mathbf{e}_{\mathbf{k}\lambda_\gamma} &= \sum_{\sigma_\gamma=0,\pm 1} \boldsymbol{\chi}^{(\sigma_\gamma)} d_{\sigma_\gamma\lambda_\gamma}^{(1)}(\theta_\gamma) e^{-i\sigma_\gamma\phi_\gamma}. \quad (52)
\end{aligned}$$

Here θ, ϕ are the angles of the vector \mathbf{p} , whereas $\theta_\gamma, \phi_\gamma$ are those of \mathbf{k} , and also $\hat{s}_z u_{\varepsilon\lambda}^{(\sigma)} = \sigma u_{\varepsilon\lambda}^{(\sigma)}$, $(\boldsymbol{\chi}^{(\sigma_\gamma)})^* \cdot \boldsymbol{\chi}^{(\sigma'_\gamma)} = \delta_{\sigma_\gamma\sigma'_\gamma}$. We also employ the phase convention of Ref. [1], so that $\hat{j}_z u_{\mathbf{p}\lambda} = 0$ (see details in [14]). The small Wigner functions are

$$\begin{aligned}
d_{\sigma\lambda}^{(1/2)}(\theta) &= \delta_{\sigma\lambda} \cos(\theta/2) - 2\sigma \delta_{\sigma,-\lambda} \sin(\theta/2), \\
d_{\sigma_\gamma\lambda_\gamma}^{(1)}(\theta_\gamma) &= \left\{ d_{\lambda_\gamma\lambda_\gamma}^{(1)} = \cos^2(\theta_\gamma/2), d_{-\lambda_\gamma\lambda_\gamma}^{(1)} = \sin^2(\theta_\gamma/2), d_{0\lambda_\gamma}^{(1)} = \frac{\lambda_\gamma}{\sqrt{2}} \sin(\theta_\gamma) \right\}, \quad \lambda_\gamma = \pm 1. \quad (53)
\end{aligned}$$

We find

$$\begin{aligned}
\bar{u}_{\varepsilon'\lambda'}^{(\sigma')} \boldsymbol{\gamma} u_{\varepsilon\lambda}^{(\sigma)} &= \left(2\lambda\sqrt{\varepsilon - m}\sqrt{\varepsilon' + m} + 2\lambda'\sqrt{\varepsilon' - m}\sqrt{\varepsilon + m} \right) \left(\omega^{(\sigma')} \right)^\dagger \boldsymbol{\sigma} \omega^{(\sigma)} = \\
&= \left(2\lambda\sqrt{\varepsilon - m}\sqrt{\varepsilon' + m} + 2\lambda'\sqrt{\varepsilon' - m}\sqrt{\varepsilon + m} \right) 2\sigma \left(\boldsymbol{\chi}^{(0)} \delta_{\sigma\sigma'} - \boldsymbol{\chi}^{(2\sigma)} \sqrt{2} \delta_{\sigma,-\sigma'} \right). \quad (54)
\end{aligned}$$

and then

$$\bar{u}_{\varepsilon'\lambda'}^{(\sigma')} \left(\chi^{(\sigma_\gamma)} \right)^* \cdot \gamma u_{\varepsilon\lambda}^{(\sigma)} = \left(2\lambda\sqrt{\varepsilon - m}\sqrt{\varepsilon' + m} + 2\lambda'\sqrt{\varepsilon' - m}\sqrt{\varepsilon + m} \right) 2\sigma \left(\delta_{\sigma_\gamma 0} \delta_{\sigma\sigma'} - \sqrt{2} \delta_{\sigma_\gamma, 2\sigma} \delta_{\sigma, -\sigma'} \right) \quad (55)$$

Summing over $\sigma, \sigma', \sigma_\gamma$, we notice that only the terms obeying $\sigma = \sigma' + \sigma_\gamma$ contribute, and so there are four of them

$$\begin{aligned} M_{fi} &= g_{\lambda\lambda'} \sum_{\sigma, \sigma', \sigma_\gamma} \delta_{\sigma, \sigma' + \sigma_\gamma} M_{fi}^{(\sigma\sigma'\sigma_\gamma)} e^{i\zeta_{fi}^{(\sigma\sigma'\sigma_\gamma)}} = g_{\lambda\lambda'} \left(M_{fi}^{(\frac{1}{2}, -\frac{1}{2}, 1)} e^{i\zeta_{fi}^{(\frac{1}{2}, -\frac{1}{2}, 1)}} + \right. \\ &\quad \left. + M_{fi}^{(\frac{1}{2}, \frac{1}{2}, 0)} e^{i\zeta_{fi}^{(\frac{1}{2}, \frac{1}{2}, 0)}} + M_{fi}^{(-\frac{1}{2}, \frac{1}{2}, -1)} e^{i\zeta_{fi}^{(-\frac{1}{2}, \frac{1}{2}, -1)}} + M_{fi}^{(-\frac{1}{2}, -\frac{1}{2}, 0)} e^{i\zeta_{fi}^{(-\frac{1}{2}, -\frac{1}{2}, 0)}} \right), \end{aligned} \quad (56)$$

where

$$g_{\lambda\lambda'} = \sqrt{4\pi\alpha} \left(2\lambda\sqrt{\varepsilon - m}\sqrt{\varepsilon' + m} + 2\lambda'\sqrt{\varepsilon' - m}\sqrt{\varepsilon + m} \right), \quad (57)$$

and the helicity amplitudes, which are real but not necessarily positive, are

$$\begin{aligned} M_{fi}^{(\frac{1}{2}, -\frac{1}{2}, 1)} &= \sqrt{2} d_{1/2, \lambda}^{(1/2)}(\theta) d_{-1/2, \lambda'}^{(1/2)}(\theta') d_{1\lambda_\gamma}^{(1)}(\theta_\gamma), & \zeta_{fi}^{(\frac{1}{2}, -\frac{1}{2}, 1)} &= -\frac{1}{2}(\phi + \phi') + \phi_\gamma, \\ M_{fi}^{(\frac{1}{2}, \frac{1}{2}, 0)} &= -d_{1/2, \lambda}^{(1/2)}(\theta) d_{1/2, \lambda'}^{(1/2)}(\theta') d_{0\lambda_\gamma}^{(1)}(\theta_\gamma), & \zeta_{fi}^{(\frac{1}{2}, \frac{1}{2}, 0)} &= \frac{1}{2}(\phi' - \phi), \\ M_{fi}^{(-\frac{1}{2}, \frac{1}{2}, -1)} &= -\sqrt{2} d_{-1/2, \lambda}^{(1/2)}(\theta) d_{1/2, \lambda'}^{(1/2)}(\theta') d_{-1\lambda_\gamma}^{(1)}(\theta_\gamma), & \zeta_{fi}^{(-\frac{1}{2}, \frac{1}{2}, -1)} &= -\zeta_{fi}^{(\frac{1}{2}, -\frac{1}{2}, 1)}, \\ M_{fi}^{(-\frac{1}{2}, -\frac{1}{2}, 0)} &= d_{-1/2, \lambda}^{(1/2)}(\theta) d_{-1/2, \lambda'}^{(1/2)}(\theta') d_{0\lambda_\gamma}^{(1)}(\theta_\gamma), & \zeta_{fi}^{(-\frac{1}{2}, -\frac{1}{2}, 0)} &= -\zeta_{fi}^{(\frac{1}{2}, \frac{1}{2}, 0)}. \end{aligned} \quad (58)$$

Finally,

$$\begin{aligned} |M_{fi}|^2 / g_{\lambda\lambda'}^2 &= \sum_{\sigma, \sigma', \sigma_\gamma} \delta_{\sigma, \sigma' + \sigma_\gamma} \left(M_{fi}^{(\sigma\sigma'\sigma_\gamma)} \right)^2 + 2M_{fi}^{(\frac{1}{2}, -\frac{1}{2}, 1)} M_{fi}^{(\frac{1}{2}, \frac{1}{2}, 0)} \cos \left(\zeta_{fi}^{(\frac{1}{2}, -\frac{1}{2}, 1)} - \zeta_{fi}^{(\frac{1}{2}, \frac{1}{2}, 0)} \right) + \\ &\quad + 2M_{fi}^{(\frac{1}{2}, -\frac{1}{2}, 1)} M_{fi}^{(-\frac{1}{2}, \frac{1}{2}, -1)} \cos \left(\zeta_{fi}^{(\frac{1}{2}, -\frac{1}{2}, 1)} - \zeta_{fi}^{(-\frac{1}{2}, \frac{1}{2}, -1)} \right) + \\ &\quad + 2M_{fi}^{(\frac{1}{2}, -\frac{1}{2}, 1)} M_{fi}^{(-\frac{1}{2}, -\frac{1}{2}, 0)} \cos \left(\zeta_{fi}^{(\frac{1}{2}, -\frac{1}{2}, 1)} - \zeta_{fi}^{(-\frac{1}{2}, -\frac{1}{2}, 0)} \right) + \\ &\quad + 2M_{fi}^{(\frac{1}{2}, \frac{1}{2}, 0)} M_{fi}^{(-\frac{1}{2}, \frac{1}{2}, -1)} \cos \left(\zeta_{fi}^{(\frac{1}{2}, \frac{1}{2}, 0)} - \zeta_{fi}^{(-\frac{1}{2}, \frac{1}{2}, -1)} \right) + \\ &\quad + 2M_{fi}^{(\frac{1}{2}, \frac{1}{2}, 0)} M_{fi}^{(-\frac{1}{2}, -\frac{1}{2}, 0)} \cos \left(\zeta_{fi}^{(\frac{1}{2}, \frac{1}{2}, 0)} - \zeta_{fi}^{(-\frac{1}{2}, -\frac{1}{2}, 0)} \right) + \\ &\quad + 2M_{fi}^{(-\frac{1}{2}, \frac{1}{2}, -1)} M_{fi}^{(-\frac{1}{2}, -\frac{1}{2}, 0)} \cos \left(\zeta_{fi}^{(-\frac{1}{2}, \frac{1}{2}, -1)} - \zeta_{fi}^{(-\frac{1}{2}, -\frac{1}{2}, 0)} \right), \\ \zeta_{fi} &= \arctan \frac{\sum_{\sigma, \sigma', \sigma_\gamma} \delta_{\sigma, \sigma' + \sigma_\gamma} M_{fi}^{(\sigma\sigma'\sigma_\gamma)} \sin \left(\zeta_{fi}^{(\sigma\sigma'\sigma_\gamma)} \right)}{\sum_{\sigma, \sigma', \sigma_\gamma} \delta_{\sigma, \sigma' + \sigma_\gamma} M_{fi}^{(\sigma\sigma'\sigma_\gamma)} \cos \left(\zeta_{fi}^{(\sigma\sigma'\sigma_\gamma)} \right)}, \end{aligned} \quad (59)$$

where the sums include only four above terms obeying $\sigma = \sigma' + \sigma_\gamma$.

On the triangle point from Eq.(46) $\phi = \phi' + \alpha, \phi_\gamma = \phi' + \alpha + \gamma$, we have

$$\begin{aligned} \zeta_{fi}^{(\frac{1}{2}, -\frac{1}{2}, 1)} &= -\frac{1}{2}(\phi + \phi') + \phi_\gamma \rightarrow \gamma + \alpha/2, \\ \zeta_{fi}^{(\frac{1}{2}, \frac{1}{2}, 0)} &= \frac{1}{2}(\phi' - \phi) \rightarrow -\alpha/2, \\ \zeta_{fi}^{(-\frac{1}{2}, \frac{1}{2}, -1)} &= \pi + \frac{1}{2}(\phi + \phi') - \phi_\gamma \rightarrow -\gamma - \alpha/2, \\ \zeta_{fi}^{(-\frac{1}{2}, -\frac{1}{2}, 0)} &= -\frac{1}{2}(\phi' - \phi) \rightarrow \alpha/2, \end{aligned} \quad (60)$$

where in the second point $\phi = \phi' - \alpha, \phi_\gamma = \phi' - \alpha - \gamma$ the phases change the signs and so

$$\zeta_{fi} \Big|_{\phi=\phi'+\alpha, \phi_\gamma=\phi'+\alpha+\gamma} = -\zeta_{fi} \Big|_{\phi=\phi'-\alpha, \phi_\gamma=\phi'-\alpha-\gamma}, \quad (61)$$

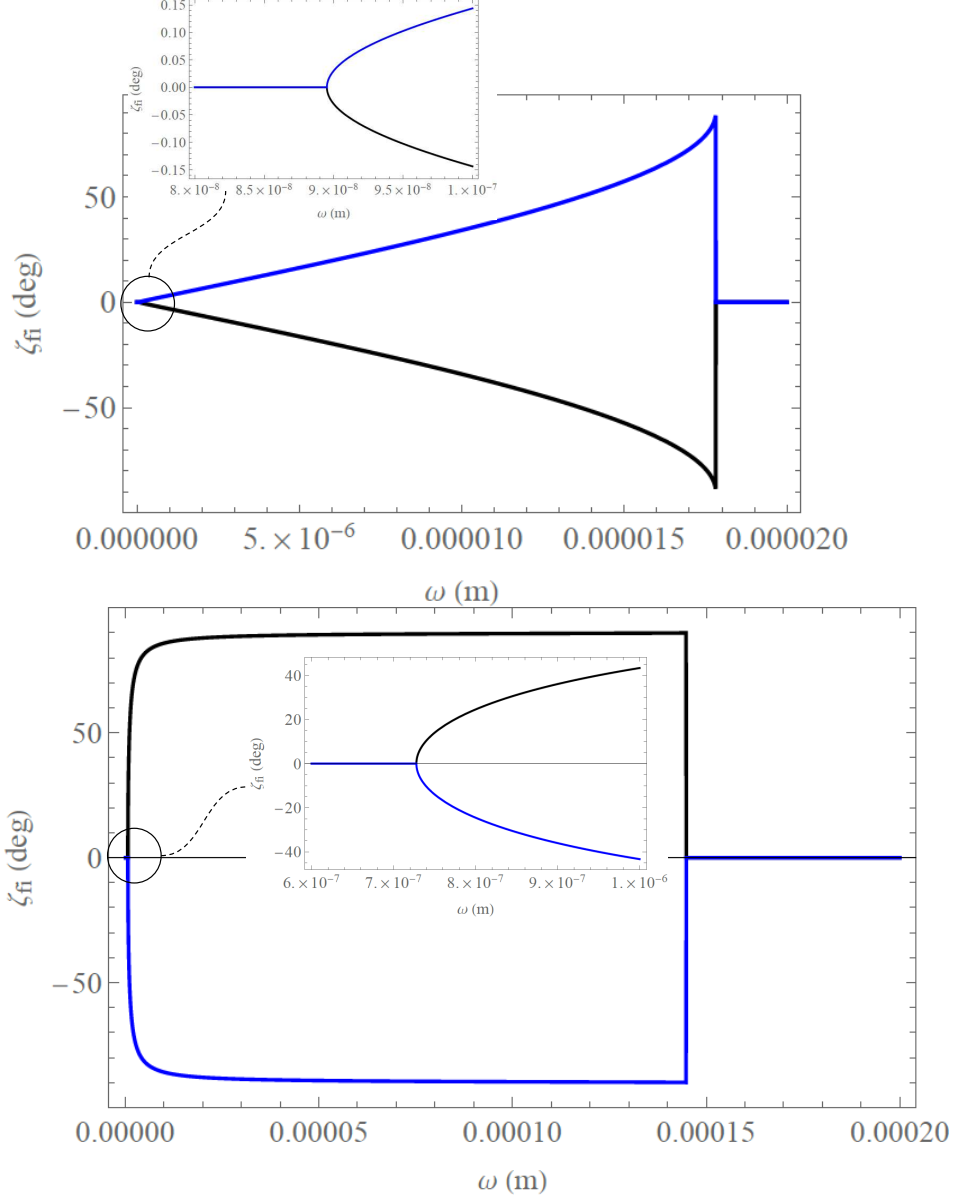


Figure 1: The phase of the scattering amplitude $\zeta_{fi} = \arg M_{fi}$ from Eq.(59) at the Cherenkov angle including the quantum recoil (44) for $\beta = 0.999$. Black line is for the first triangle point from Eq.(46), whereas the blue one is for the second point. Upper panel: $n = 1.5, p_{\perp} = 10^{-5}m, p'_{\perp} = 0.99 \times p_{\perp}, p'_z = 0.99 \times \beta, \lambda = \lambda' = 1/2, \lambda_{\gamma} = \pm 1$. Lower panel: $n = 1.7, p_{\perp} = 10^{-4}m, p'_{\perp} = 0.99 \times p_{\perp}, p'_z = 0.99 \times \beta, \lambda = -\lambda' = 1/2, \lambda_{\gamma} = \pm 1$. When $\lambda = -\lambda' = -1/2$, the black and blue lines swap.

whereas

$$|M_{fi}|^2 \Big|_{\phi=\phi'+\alpha, \phi_\gamma=\phi'+\alpha+\gamma} = |M_{fi}|^2 \Big|_{\phi=\phi'-\alpha, \phi_\gamma=\phi'-\alpha-\gamma}. \quad (62)$$

Thus, the phase changes the sign for two momentum configurations from Eq.(46) together with the quantum shift in the photon arrival time depending on the phase derivative, whereas $|M_{fi}|^2$ does not. Note that the phases – and so the matrix element – do not depend on the azimuthal angle of the final electron momentum ϕ' . The transverse momenta in the amplitudes must satisfy the triangle rules Eq.(48).

In Fig.1 we show that the phase is not constant even at the tree-level and it is non-vanishing in a finite region of momentum space defined by the momentum conservation law. The region of frequencies $\Delta\omega$ for which the phase and its derivative stay non-vanishing defines the magnitude of the quantum shift in the photon arrival time, discussed in the main part of the manuscript.

References

- [1] V. Berestetskii, E. Lifshitz, and L. Pitaevskii, *Quantum Electrodynamics* (Butterworth-Heinemann, 1982).
- [2] M. Peskin and D. Schroeder, *An introduction to quantum field theory* (Westview Press, 1995).
- [3] M. Scully and M. Zubairy, *Quantum optics* (Cambridge university press, 1997).
- [4] W. P. Schleich, *Quantum optics in phase space* (John Wiley & Sons, 2015).
- [5] I. Ivanov, V. Serbo, and V. Zaytsev, *Physical Review A* **93**, 053825 (2016).
- [6] D. Karlovets, *Journal of High Energy Physics* **2017**, 1 (2017).
- [7] G. Antchev *et al.*, *The European Physical Journal C* **76**, 1 (2016).
- [8] D. V. Karlovets and V. G. Serbo, *Physical Review D* **101**, 076009 (2020).
- [9] V. Bagrov, V. Belov, and A. Trifonov, *Journal of Physics A: Mathematical and General* **26**, 6431 (1993).
- [10] V. A. Verzilov, *Phys. Lett. A* **273**, 135 (2000).
- [11] A. P. Potylitsyn *et al.*, *Diffraction Radiation from Relativistic Particles*, STMP Vol. 239 (Springer, Berlin Heidelberg, 2010).
- [12] I. Kaminer *et al.*, *Physical Review X* **6**, 011006 (2016).
- [13] K. Bliokh *et al.*, *Physics Reports* **690**, 1 (2017).
- [14] D. Karlovets, S. Baturin, G. Geloni, G. Sizykh, and V. Serbo, *The European Physical Journal C* **83**, 372 (2023).